Nanoscale

Accepted Manuscript

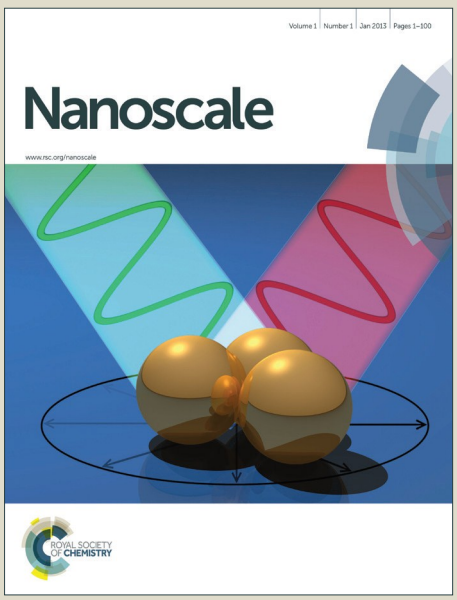

ROYAL SOCIETY OF CHEMISTRY

www.rsc.org/nanoscale

Nanoscale

REVIEW

The relevance of membrane models to understand nanoparticles-cell membrane interactions

Estelle Rascol,[a] Jean-Marie Devoisselle[a] and Joël Chopineau *[a,b]

During the two past decades, numerous types of nanoparticles (NPs) have been developed for medical applications; however only a few nanomedicines are actually available on the market. One reason is a lack of understanding and data concerning the NPs fate and their behavior upon contact with biological media and cell membranes. Biomimetic membrane models are interesting tools to approach and understand NPs-cell membrane interactions. The use of these models permits to control physical and chemical parameters and to rapidly compare membranes types and the influence of different media conditions. The interactions between NPs and cell membranes can be qualified and quantified using analytical and modeling methods. In this review, the major studies concerning NPs-cell membrane models and associated methods are described. The advantages and drawbacks for each method are compared for the different models. Key mechanisms of interactions between NPs and cell membranes are revealed using cell membrane models and are interrogated in comparison with NPs behavior in *cellulo* or *in vivo*. Investigating the interactions between NPs and cell membrane models is now proposed as an intermediate step between physicochemical characterization of NPs and biological assays.

Received 30th October 2015,
Accepted 00th January 20xx

DOI: 10.1039/x0xx00000x

www.rsc.org/

Introduction

Nanomaterials are defined as materials containing particles or nano-objects of at least one external dimension in the size range of 1 to 100 nm (from 2011/696/UE recommendations).[1] Nanometer scale confers special physicochemical properties to matter and materials. When material size decreases, the surface to volume ratio is increased, with a majority of molecules at the surface of the object, inducing an increased surface reactivity.[2] Then optical, magnetic, thermal, mechanical, catalytic or electronic properties of materials are modified due to the nanometer scale.

These properties are of noticeable interest and relevant for biomedical applications, such as: imaging, diagnosis, drug-delivery, or cell-targeting.[3] In 2013, 230 products classified in the nanomedicine field were sold on the world market.[4] According to the registry maintained by clinicaltrials.gov, a total of 1828 nanomedicine formulations (search terms “liposome” OR “nanoparticle” OR “micelle” OR “nanocrystal”) had been registered for clinical trials by first September 2015. 95 of these are in phase 4, which recently reached the market.

The biological activities and toxic effects of particles are governed by the nature and the physicochemical properties of the particles (Fig. 1). Also, an important role is played by particle surface properties for NPs biological behavior and fate. NPs size is not the only parameter to take into account to investigate biological outcome.

[a] *Institut Charles Gerhardt, UMR 5253 CNRS/ENSCM/UM, 8 rue de l’Ecole Normale, 34296, Cedex 5 Montpellier*
[b] *Université de Nimes Rue Georges Salan, 30000 Nimes, France.*

* Corresponding author E-mail Joel.Chopineau@enscm.fr
Electronic Supplementary Information (ESI) available: [details of any supplementary information available should be included here]. See DOI: 10.1039/x0xx00000x

Aggregation/agglomeration, shape, porosity, surface area, surface charge, crystalline material form and dissolution properties must also be well characterized.[5] Upon contact of NPs with biological fluids, several forces are involved at the interface between NPs and the liquid medium.[6] These forces governing the interactions are similar to those observed for colloidal particles, with some differences due to the nanoscale. They are hydrodynamic, electrodynamic, electrostatic, solvation, and steric interactions; implying plasma pH, temperature, ions, proteins, and oxidative species. DLVO (Derjaguin-Landau-Verwey-Overbeek) theory considers the sum of these forces for the understanding of NPs behavior.[6]

After intravenous injection (the main route for administration of NPs) plasma proteins will interact directly and rapidly with the NP surface, leading to a protein corona.[7] Then, this corona may change different NP properties compared to pristine ones (hydrodynamic diameter, surface charge, aggregation, etc). The primary protein-corona composition is dependent on the bare NPs properties, such as size or surface chemistry. The presence of the corona will influence NPs biological behavior.[8, 9] Corona proteins contain opsonins (non-specific antibodies and complement proteins) responsible for white blood cells and macrophage recognition, leading to NPs opsonization.[10] During this process, NPs are removed from the plasma by macrophages through phagocytosis. Other cell types internalize NPs by slower mechanisms. NPs might penetrate cells by passive translocation or endocytosis pathways. Passive translocation has been observed for NPs penetration into red blood cells (RBC), which are devoided of an active internalization system.[11] Negative and neutral particles with a size of up to 0.2 µm were found in RBCs while positively charged and 1 µm NPs were only found attached to the cell membrane.

During active endocytosis, NPs bind to the cell membrane, for example via corona proteins recognized by membrane receptors. Cell membranes invaginate surrounding NPs via intra- or extra-cellular proteins, depending on the endocytosis pathway involved. Four main endocytosis pathways are described for NPs internalization.[12] Phagocytosis is performed only by specialized cells, macrophages, and result in the formation of relatively large vesicles (> 500 nm). Pinocytosis is a non-specific mechanism, leading to large intra-cellular vesicles (0.5-5 µm). Conversely, calveolae and clathrin-mediated endocytosis pathways allow internalization of NPs, within vesicles of sizes 60-80 nm and 100-120 nm, respectively. NPs physicochemical properties are involved in intracellular trafficking of NPs too, due to the different internalization pathways involved.[13]

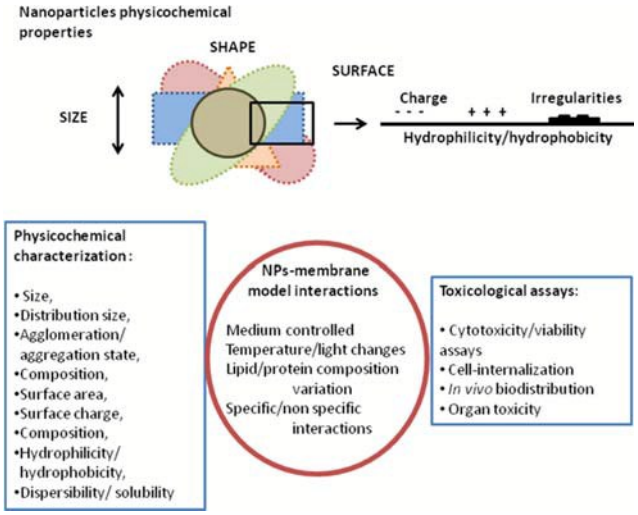

Fig. 1 : Physicochemical NP properties influencing biological behaviour. NP size, shape and surface properties significantly influence biological activity and toxic effects. These characteristics impact protein corona composition, body distribution, cell membrane attachment, and the penetration process. Membrane models allow cell membrane mimicking in controlled conditions, such as medium composition (pH, ionic strength, the absence or presence of proteins). The model membrane composition can also be changed in terms of lipid or protein content to get closer to a cellular type or organelle membrane composition. The impact of external parameters such as temperature and light exposure may also be examined. Specific and non-specific interactions are evidenced using these different tools. A membrane model may be used in complement to physicochemical characterization, and to prevent toxicological assay artifacts.

The main toxic effects of NPs result from their interactions with cellular components such as the plasma membrane, organelles, or macromolecules.[14] These interactions are largely dependent on complexity and varying size, shape, charge, chemical composition, surface functionalization or aggregation tendency (Fig. 1). Major cytotoxic effects observed result in reactive oxygen species (ROS) generation that will cause lipid peroxidation, inflammatory response, or DNA (Desoxyribo Nucleic Acid) damage. Physicochemical properties of NPs are well described as critical factors in the toxic effects induced by NPs exposure. In comparison to complex biological media, membrane models provide useful systems to investigate NPs membrane interaction and their role on the NP cytotoxicity. So it became unavoidable to use membrane models to understand the interrelation between NPs and biological membranes.[12]

Membrane models are simplified systems in which almost all physical and chemical parameters can be controlled. They are particularly interesting for a systematic characterization of membrane attachment and disruption by NPs, and to visualize NPs-membrane interactions.[15] To this goal, three major membrane models are relevant for NPs-cell membrane interactions studies: lipid vesicles or planar lipid models, and more recently modelisation models (Fig. 2). These different membrane models are frequently associated with various methods providing complementary data.

Biological membranes are composed of typical lipids, associated with functional proteins such as receptors, ion channels, glycoproteins.[16] Phospholipids, associated or not with membrane proteins, cholesterol, or other membrane lipids compose experimental membrane models. It remains difficult to investigate the behavior of nano-objects when they are in contact with biological fluids, cells .., such as cell internalization process and biodistribution. These different models contribute to the comprehensive link between NPs physicochemical properties and toxic effects. In this review, different biomimetic membrane models and their application for NPs interactions analysis will be described. The relevance of membrane models and associated methods for NPs cell membrane interactions monitoring will be presented, along with their advantages and drawbacks.

Membrane models and associated methods

Lipid vesicles

Biological membranes are composed of typical lipids (phospholipids (glycero-, sphingo-, glyco-); cholesterol), associated with functional proteins such as receptors, ion channels, pumps … .[16] Due to the complexity of membrane composition and architecture, model membrane systems were introduced in the 60's.[17]

Model description

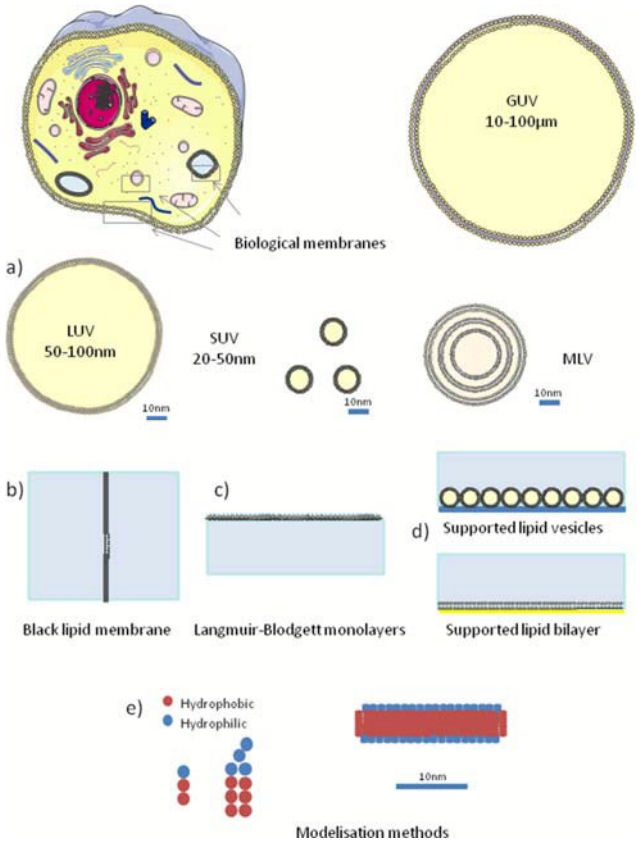

Fig. 2 : Major membrane models used to understand NPs-cell membrane interactions. Membrane models such as lipid vesicles (a) or planar lipid models (b, c, d) are completed by recently developed modelisation methods (e). Lipid vesicles which include giant unilamellar lipid vesicles (GUV), small (SUV), large (LUV) or multilamellar vesicles (MLV), are spherical vesicles delimited by a phospholipid bilayer separating two aqueous compartments. GUVs are 10 to 100 µm in size, 10 µm GUVs are in the size range of eukaryote cells, including a membrane curvature close to the cell's one. Lipid vesicles could be studied on planar surfaces, as supported lipid vesicles. Three major planar lipid models are relevant to study NP-cell membrane interactions. Black lipid membrane is a 150-200 µm diameter free lipid bilayer separating two aqueous compartments that is particularly useful to study membrane electric properties upon NPs exposure (b). The Langmuir-Blodgett monolayer is a lipid layer at the air-water interface (c). Lipid parameter measurements such as lipid surface area bring lipid packing information. Supported lipid bilayers may be formed on different materials, mainly driven by the associated analytical methodologies. For modelisation methods, lipids are represented by all lipid atoms or just some beads (e). These different membrane models are frequently associated with various physicochemical methods for data acquisition.

Liposomes are spherical vesicles delimited by a phospholipid bilayer separating two aqueous compartments. This configuration offers the possibility for loading hydrophilic compounds into the internal aqueous compartment while hydrophobic compounds could be inserted into the lipid bilayer. The vesicles could be delimited by one (unilamellar vesicle) or by multiple bilayers (multilamellar vesicle). They could be small (20-50 nm), large (50-100 nm), or giant (10-100 µm) unilamellar vesicles (Fig. 2a), they are named SUVs, LUVs, GUVs, respectively.[18] These models are already considered as the simplest membrane models to investigate xenobiotic (substance that is foreign to the biological system) toxic effects on biological membranes.[19] Different research groups are using lipid vesicles as tools to investigate the role of membrane lipids upon interactions of NPs with biological membranes.

Methods

Vesicle visualization is possible using light microscopy or polarized light microscopy.[20] However, the resolution is about 200 nm. This technique is only relevant to observe GUV, and images don't allow a good definition of the object. An alternative to observe GUV is by use of fluorescent microscopy (Fig. 3b). An epifluorescence inverted microscope could be used, [21] but a confocal microscope has a better definition.[22] Fluorescent molecules could be internalized into the lipid vesicle or attached to phospholipids. Better microscopic vesicle observations can be performed using transmission electron microscopy (TEM), which has a resolution about 0.2 nm. Vesicle observation requires a negative stain step, using uranyl acetate or osmium tetroxide.[20] Because of artefacts potentially caused by sample staining, fixation or dehydration, cryogenic TEM has been developed. The resolution is about 1-2 nm at 200kV,[23] and the sample is size-limited to 500 nm due to the freeze film thickness. The cryo-preserved samples could be observed using fracturing techniques. These methods offer visualization of bilayer arrangement, the different phases, which is particularly interesting for multilamellar vesicles observation. Finally, environmental scanning electron microscopy (ESEM) is performed without fixation, staining, dehydration or freezing, and offers vesicle observation into its medium. Modification of vesicle morphology in response to

environment or pressure changes can be observed in real-time. To observe NPs-vesicle interaction, mainly fluorescent techniques and cryoTEM have been used.[21, 22,23]

A simple method, firstly described in 1977, used to decipher the interactions of NPs with lipid membrane models is the dye leakage assay.[24] In this method, the liposomes are loaded with a hydrophilic molecular probe that is encapsulated in the internal aqueous compartment. Following the interactions of NPs with the membrane, defects may occur in the lipid bilayer causing the release of the molecular probe from the liposome. This test was firstly used to investigate gold NPs (AuNPs) cell membrane interactions in 2004 (Fig. 3a).[25]

During the 70's, another fluorescent method was developed in parallel, the fluorescence recovery after photobleaching (FRAP). This technique is based on fluorescent bleaching of fluorescent molecules when exposed to white light.[26] Then, fluorescent lipids are mixed with lipids composing of vesicles which can be observed using confocal microscopy. During FRAP experiments, fluorescent lipids are locally bleached by light. Images of fluorescence recovery as function of time could be recorded. Because of lateral lipid mobility, the bleached zone recovered fluorescence again (Fig.3c). Analyses of these data allow the determination of lateral mobility of lipids and their diffusion coefficients, which are characteristic parameters of biological and model membranes. The interaction of nano-objects with membranes will impact these physicochemical parameters.

Another fluorescent lipid-based assay, the Laurdan (6-lauryl-2-(N,N-dimethylamino) naphtalene) assay, is sensitive to lipid physical states, such as packing or hydration of phospholipids heads. Upon excitation at 780 nm, this fluorescent probe has two emission maxima, 440 and 490 nm. An increase in fluorescence intensity (IF) 440nm peak with respect to the 490 nm peak is related to a membrane that is more ordered and less hydrated, also the ratio IF 440/IF490 is a qualitative indicator of lipid packing and hydration.[27]

Interaction of membrane lipids with xenobiotics could induce physical perturbations of the lipid membrane. For example, the melting transition temperature of lipids (Tm) is currently modified. These Tm changes are measured using dynamic scanning calorimetry (DSC). DSC measures heat release (exothermic reaction) and heat absorption (endothermic reaction) which are recorded on thermograms thus characterizing lipid physical state, such as fluid or gel phase. DSC is a method largely used to investigate xenobiotic toxic effects using a lipid vesicles as membrane models.[19]

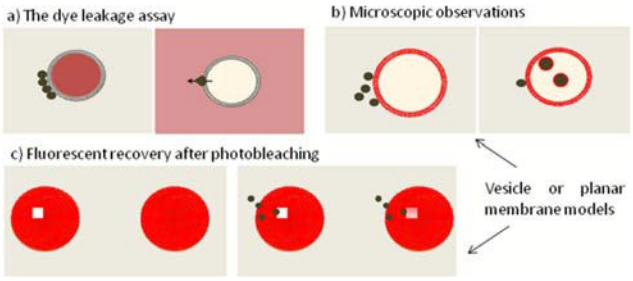

Fig. 3 : Associated vesicle membrane model methods

a) Confocal fluorescent microscopy allows observations at the nanoscale level. Lipid vesicles doped with fluorescent lipids are put in the presence of fluorescent (or non-fluorescent) NPs. Depending on their size, NPs penetrate lipid vesicles by an endocytosis-like mechanism. These mechanisms are also observed by cryo-TEM. Its higher resolution brings more precise observation details and fewer artefacts than with confocal microscopy.

b) The dye leakage assay tests the permeability of the lipid vesicles. To test permeability, a molecular probe is encapsulated into the internal aqueous compartment. If NPs induce lipid bilayer permeation, fluorescence will be detected in the external aqueous compartment. This might occur when several NPs aggregate into the lipid bilayer to form a pore or when a porous NP crosses the lipid bilayer.

c) Fluorescent recovery after photobleaching (FRAP): FRAP is currently used to characterize lateral lipid mobility and lipid bilayer fluidity. Fluorescent lipids are locally bleached with white light. Lipid mobility induces a rapid mix of bleached and fluorescent lipids refilling the bleached area. During the NP's exposure, the lipid bilayer properties may change, such as a decrease of the lateral lipid mobility. FRAP measurements could be performed either with vesicle or planar membrane models. Supported lipid bilayers (SLBs) prepared by vesicle fusion, are used to compare surface plasmon resonance (SPR), atomic force microscopy (AFM), and quartz crystal microbalance with dissipation monitoring (QCM-D) methods. SLB formation is schematized using four steps: 1) planar support without lipids, 2) lipid vesicles deposition on the top of the solid surface, 3) lipid bilayer fusion by lipid vesicles disruption, 4) interaction with NPs.

Main data obtained

Main effects observed by NPs-lipid vesicle membrane model studies are described, using the following methods: microscopic observations, dye leakage assays, FRAP experiments, Laurdan assay and DSC studies.

NPs localization and internalization in cell mimics could be evidenced by using microscopy techniques. Cryo-transmission electron tomography is an interesting tool to reconstruct NPs-lipid vesicle interaction time set.[23] To investigate NPs size effects, 1, 2-dioleoyl-phosphatidylcholine (DOPC) LUV were put in contact with 15, 30, 40, 65, 190 nm diameter maghemite nanocrystals core shell silica NPs ($\gamma Fe_2O_3@SiO_2$). Smaller NPs (about 15 nm diameter), remained bound to the outer surface, unlike NPs larger than 30 nm that were entrapped in the liposome. During the entrapment process, NPs were firstly attached to the vesicle; they were surrounded by the lipid bilayer and finally released into the internal compartment of the vesicle. NPs that were wrapped in the lipid bilayer were not able to interact further with other vesicles. The internalization process was demonstrated to be a size dependent process.

The interaction of 2 nm AuNPs with cells and the resulting toxicity was observed into three cell types(Cos-1 cells, red blood cells, *Escherichia coli* cultures) each with different membrane properties.[25] In order to explain the cytotoxicity results obtained on different cell lines, dye leakage assays using model vesicles were performed. Vesicle leakage assay was achieved using lipid vesicles formed with L-α-stearoyl-oleoyl-phosphatidylcholine (SOPC) (neutral lipid) or a mix SOPC/SOPS (L-α-stearoyl-oleoyl-phosphatidylserine) (negatively charged). Amino functionalized (cationic) and carboxy- functionalized (anionic) AuNPs were tested

for dye leakage with the vesicles of each composition. The cationic AuNPs induced the release of more dye than anionic ones. This was an argument to prove that eukaryote cell toxicity of gold NPs is associated to direct interaction with cell membrane by electrostatic attraction.

The comparison of titanium (TiO_2 NPs) and AuNPs core coated with different chemical groups interacting with lipid vesicles , using the leakage assay, was recently reported.[28] TiO_2 NPs and AuNPs were both functionalized with DAD (diallyldiammonium) groups. Other TiO_2 NPs and AuNPs were respectively coated with sodium polyacrylate and tannic acid or poly(vinylpyrrolidone). These different coatings resulted on differently charged NPs but little variation in hydrodynamic diameter. Zwitterionic DOPC liposome leakage was found to occur with these 10 nm NPs. Analyses of TEM images showed that the presence of only one particle per liposome was able to induce leakage of the probe. Cationic AuNPs and TiO_2 NPs coated with DAD groups were found to induce liposome leakage. The cationic group by itself was not able to induce significant leakage confirming that leakage was caused by NPs coated with this cationic group on the surface.

The role of electrostatic attraction between NPs and lipid bilayers was also investigated using liposome leakage assay associated with other methods (reflectometry assay and modelisation).[29] Silica (8 nm) and titanium (5-15 nm) oxide NPs were put in contact with various charged lipids DOPC/DOPG (1, 2-dioleoyl-phosphoglycerol) and at different ratios. Electrostatic interactions were also evidenced through the variation of pH from 4 to 10.

Confocal microscopy was used to decipher the mechanism of NP interaction with the lipid bilayer by Laurencin et al.[30] Their results provided evidence that NPs charge coverage was involved in the non-specific interactions of NPs with the membrane. The membrane composition was varied to study NP interaction with positive, negative or neutral lipids. Using fluorescent lipids and NPs, the easy use of confocal microscopy provides rapid information on NP localization, binding or internalisation of NPs in vesicles.

The same method was used by Zhang et al.,[22] to understand the impact of the NPs size on membrane interactions. 18, 78 and 180 nm silica NPs were compared on a GUV model. GUV was produced by electroformation with DOPC lipid containing 0.5 mol% fluorophores (LissRhodPE). By confocal microscopy, two different interaction mechanisms were observed for larger and smaller NPs. 18 nm NPs seemed to attach to the vesicle surface, inducing leakage and stabilised holes into the lipid bilayer. On the contrary, membrane wraps appeared around 180 nm NPs. More detail about lipid properties, such as lipid lateral mobility and membrane fluidity were obtained by FRAP analysis.[22] When GUV interacted with 18 nm NPs, lateral mobility was reduced, attributed to a fluid-to-gel phase transformation called as “freeze effect”. On the contrary, GUV exposure to 78 and 180 nm NPs showed an increased lateral diffusion suggesting defects in the GUV, associated with a wrapping mechanism. These observations suggested a different mechanism was used for 18 nm NPs and the larger ones.

Lipid physical state, as packing or hydration, was obtained by Laurdan assay. In the study of Churchman et al.[31] a combination of three fluorescent methods were used: leakage assay, labelled GUV and Laurdan assay (6-dodecanoyl-2-dimethylaminonaphthalen). The association of the three methods show the effect of a protein corona on the interaction of NPs with a membrane model. Coating NPs with bovine serum albumin (BSA) induces a stabilization of the NP dispersion, causing them to interact more with the membrane model. This results in lipid vesicles with less hydrated and more ordered lipids, which cause a stiffening of the membrane model.

This “gellation” effect of vesicles induced by the presence of NPs has been shown using Laurdan assay, associated to Förster resonance energy transfer (FRET) and isothermal titration calorimetry (ITC). The gel-to-fluid phase transition was investigated using vesicles composed with: DOPC (Tm = - 20°C), DLPC (1,2-dilauroyl-sn-glycero-3-phosphocholine) (Tm = - 1°C) and DPPC (Tm = 40°C). Latex polystyrene NPs with a diameter of 20 nm with carboxyl (anionic) or amidine (cationic) modified surfaces were placed in suspension with the vesicles and their effects on vesicles were analyzed. On the one hand, anionic NPs induced a local “gellation” effect of the lipid membrane, independently of lipid nature or vesicle size. On the other hand, cationic NPs induced a fluidization of lipids in gel phase but negligible effect on lipids in the fluid phase was observed.[32] Tm changes were observed after lipid vesicle interaction with silica NPs (100 nm) by DSC measurements.[33] Liposomes composed of 1, 2-dimyristoyl-*sn*-gycero-3-phosphocholine (DMPC), or 1, 2-dimyristoyl-3-trimethyl-ammonium-propane (DMTAP), or an equal mixture of both, measured 110-190 nm. The calorimetric thermograms of lipid vesicles by themselves or NPs surrounded these lipid vesicles in different NP/lipid ratios, were recorded and compared. Results presented by these authors showed that the Tm decreased when the lipid vesicle was in contact with NPs. Plus, when lipid vesicles were in excess, DSC thermograms showed a Tm of lipid vesicles wrapping NPs different from the Tm of free vesicles. Similar results were obtained with another nano-object, fullerene. The interactions of fullerene with large unilamellar vesicles (150-180 nm) formed with phosphatidyl choline (PC) or DMPC, with or without cholesterol were investigated with the DSC method.[34] The different formulations showed a slight decrease in Tm when vesicles were in contact with fullerene. DSC measurements associated with hydrodynamic and zeta potential results suggested an incorporation of fullerenes into liposomes. These results were in accordance with results obtained by the study of SiO_2 NPs-lipid vesicle interaction. The Tm decrease was only observed when the lipid bilayer was in contact with the NP. This suggests that the gel to liquid transition change was due to stabilization of the lipid bilayer. NPs were associated with different acyl chains, and induced packing, leading to less interaction with water molecules.

Advantages and drawbacks

Vesicles are lipid membrane models that are easy to handle and suitable for different techniques (microscopy, fluorescence,

surfaces sensitive techniques...). These models allow visualization and localization of NPs; different methods provide data concerning lipid physical state (fluidity, fluid-gel phase transition), or membrane permeability. Altogether, they provide NP lipid membrane interaction mechanisms. Unfortunately, mostly visual and qualitative data are obtained. Whilst DSC is an efficient method for knowing if lipid bilayers surround NPs, it is little used to understand the interaction mechanism between NPs and the cell membrane. Plus, to perform DSC measurements, a high concentration of lipids is needed.[19] Another major drawback is the lack of quantification of NPs interacting with a single vesicle.

Supported lipid bilayers (SLB)

Model description

SLB are planar bilayers formed on top of a solid surface (Fig. 4A). The nature of the solid support is largely dependent on the analytical methods: SPR (surface plasmon resonance) requires a thin noble metal layer (gold, silver), optical techniques require transparent surfaces (silica, quartz, glass) and AFM (atomic force microscopy) needs atomically flat surfaces (mica, silicon, flat gold).[35, 36] They are mainly used to investigate NPs-membrane attachment because some surface sensitive methods can be associated.

SLB could be formed by different routes such as Langmuir-Blodgett (LB) or Langmuir-Schaefer (LS) techniques, or by lipid vesicle fusion. LB and LS techniques are particularly interesting for the formation of asymmetric SLB. The lipid vesicle fusion on a solid support is a simple procedure to prepare SLB.[37, 38]

To mimic the cell membrane structure, numerous biomimetic membranes models have been developed using solid supports. These biomimetic membranes include solid-supported bilayer lipid membrane (Fig. 4Aa), polymer-cushioned membranes (Fig. 4Ab), hybrid bilayer lipid membrane (Fig. 4Ac) and tethered bilayer lipid membranes (Fig. 4Ad). [35, 36]

Methods

One surface-sensitive analytical method associated to the SLB model is SPR (Fig. 4Ba). The SPR phenomenon is related to the plasmonic properties of a noble metal. A thin noble metal layer, less than 50 nm in thickness, shows energy absorption properties. The resonance phenomenon is sensitive to the dielectric constant of the medium at the vicinity of the metal layer, called sensor. The first application of an SPR-based sensor was reported by monitoring biomolecular interactions in 1983.[39] SPR analyses are label-free, fast, specific, sensitive and in real-time. This method was adapted to study NPs- membrane interaction. SLB was formed on a gold chip and the interaction of NPs with the lipid bilayer was monitored by the recording of the refractive index (RI) shift. SPR is particularly relevant for studying specific interactions.[40]

AFM allows the morphology of biological samples to be recorded, in real-time and at a nanoscale resolution. In this method, the sample is set up on a piezoelectric sensor (Fig.4Bc). The force interacting between the tip and the sample is scanned with piconewton sensitivity. The solid support should be in a different but atomically flat material.[37]

At the moment, the most commonly used method to monitor NP-membrane interactions is the quartz crystal microbalance with dissipation monitoring technique (QCM-D) (Fig. 4Bb). This technique is based on the mechanical resonance of piezoelectric single crystalline quartz. A thin circular disc is sandwiched between a pair of metal electrodes. An external electric field induces a mechanical tension, which then induces an oscillating movement characterized by its frequency.[41] The frequency is changed when the mass increases on top of the sensor. The mass adsorbed on the surface is deduced from frequency changes by modelisation. This explains the sensitivity weighing of this device. The crystalline quartz support can be covered by different materials. So, it is possible to form SLB (or supported lipid vesicles) on this surface and measure the NPs interactions by mass changes. Plus, this method provides data about viscoelastic properties, by the dissipation monitoring technique.

The SLB model was also used to characterize NPs effects on the lipid bilayer when NPs are attached to the bilayer. To this goal, NPs were directly tethered to the lipids forming the bilayer.[42] NPs movements were followed using single-particle tracking (SPT). Upon tracking NPs, the effects of NPs in the immediate lipid environment, or between NPs themselves could be observed. Moreover, the mobility of NPs could also be controlled under application of an electric field.

The interferometric scattering microscopy (iSCAT) implemented using a home-built inverted optical microscope enable to detect weak scattering signals from very small domains (20 nm) using 20 nm gold NPs.[43] This system allows very sensitive SPT measurements with 1.9 nm spatial precision and 1 ms temporal resolution.

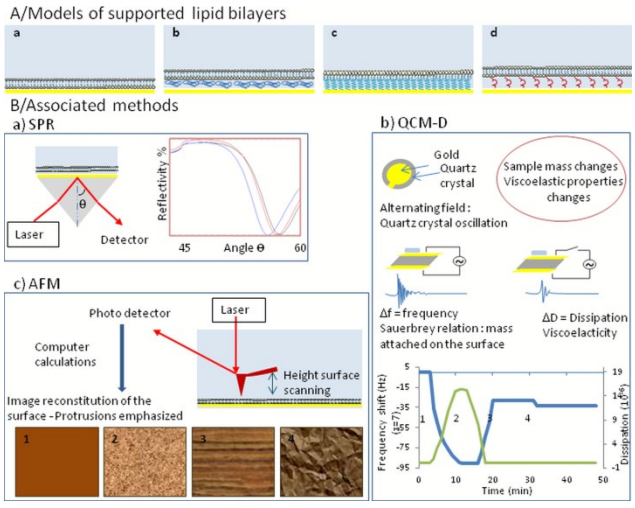

Fig. 4: Supported lipid bilayer models and major associated methods

A/The models of supported lipid bilayers include solid-supported bilayer lipid membrane (a), polymer-cushioned membranes (b), hybrid bilayer lipid membrane (c) and tethered bilayer lipid membranes (d).

B/ The major associated methods are SPR (a), QCM-D (b) and AFM (c).

a) SPR: At the resonance angle, all light energy is absorbed by the gold surface. In the angle mode, recording of the variations of reflectivity as a function of the incidence angle monitor the shift of the resonant angle upon the adsorption of material on the gold surface. Real-time and quantitative data concerning interactions at the nanoscale are obtained.

b) QCM-D: Frequency recording allows the quantification of mass on the surface that can be calculated according to the Sauerbrey relation, while dissipation depends on viscoelastic properties. SLB formation followed by NP exposure is monitored by QCM-D. The different steps are: 1) crystal quartz frequency and dissipation 2) QCM-D recordings show an increased dissipation due to the soft state of the lipid vesicles attached, while frequency decreases to an enhanced mass at the surface, 3) during lipid bilayer fusion by lipid vesicles disruption, surface is smoothed and dissipation returns to the baseline, 4) interaction with NPs induces frequency decrease due to an enhanced mass when NPs adsorb on the surface.

c) AFM: The force interacting between the tip and the sample is scanned with piconewton sensitivity. The force fluctuation is transmitted by laser to a photodetector, and after computer calculations, an image provides a projection of the reconstituted surface. The different steps for the formation of SLB and interaction with NPs are followed by schematic images close to what is observed by AFM. 1) the gold sensor alone provides a plain image, 2) lipid vesicle deposition on the top of the solid surface leads to numerous clearer points which correspond to lipid vesicles, 3) A striated image is obtained after lipid bilayer fusion by lipid vesicles disruption, 4) interaction with NPs may induce some protrusions, which are observed thanks to AFM resolution.

Main data obtained

Specific interactions have been monitored by SPR between NP protein corona and some receptors.[44] 50 nm anionic methyl methacrylate NPs were incubated with human plasma for 1h at 37°C. NPs, with or without protein corona, were put in contact with SLB for comparison. The lipid bilayer composition was largely varied, from a cholesterol sphingomyelin matrix associated with or without cardiolipin, dimyrylstoylphosphatidic acid (DMPAC), PC and monosialoganglioside GM1. Three membrane receptors were associated onto the model membrane to assess protein corona interactions, recombinant low-density lipoprotein receptor-related protein-1 (LRP-1), anti-apolipoprotein E antibody (ApoE-Ab), and anti-human albumin antibody (HAS-Ab). Just NPs covered with protein corona were able to interact with membrane receptors. In contrast to lipid-based membrane models, the results observed here showed the specificity of NP membrane interactions.

The SLB disruption mechanism could be observed thanks to the AFM method. Depending on the NP type, two different disruption mechanisms were observed: nanoscale hole formation or membrane thinning. Numerous cationic NPs have been tested on SLB by AFM to investigate if these mechanisms are frequently observed in NP-membrane model interactions.[45] Cationic charges density was not the major factor influencing NP-membrane interactions. Surface area was considered as a better predictor with a greater surface area inducing more NP-membrane interactions. The impact of lipid choice was highlighted on the results of Spurlin et al.[46] C60 are more attracted to cationic lipids than zwitterionic ones, and they form aggregates on the surface of cationic lipids. Biological membranes comprise of a lot of different lipids, characterized by headgroup charge, tail length, and phase transition temperature. This study demonstrated that NPs membrane interactions involve only lipid headgroups as bilayer thickness and phase-transition temperature modifications were not observed. Larger NPs (> 20 nm) allow the formation of a SLB around the NP whereas smaller NPs (< 20 nm) form holes during SLB formation on the surface support.[18, 47]

Passive NP insertion into the SLB was observed by association of QCM-D with AFM.[48] The combination of both techniques provide the proof of passive insertion of gold NPs with a core size of 5-6 nm coated with 11-mercapto-1-undecanesulfonate (MUS) and 1-octanethiol groups (OT) in a stoichiometric ratio of 1:1 MUS:OT.[49] The interesting result was that this passive insertion of these small NPs in the lipid bilayer occurred on defects or protrusion sites of the lipid bilayer. The hydrophobic surface of gold NPs do not insert in perfectly planar, defect-free SLB. With QCM-D, it was shown that NPs interact differently depending on lipid composition. Thus, graphene oxide didn't adsorb on the negatively charged lipid model but did with positively charged ones. This demonstrated predominant electrostatic interactions between graphene oxide and model lipid membranes. Plus, graphene oxide were able to induce liposome ruptures when preadsorbed on a planar surface (graphene oxide, gold).[48] On the other hand, DOPC lipid vesicles and SLB, deposited on QCM-D gold sensor were not disrupted by multiwalled carbon nanotubes (MWNT).[50]

Advantages and drawbacks

The main advantage of SLB is the ease in significantly varying the lipid composition. It provides the study of specific or non-specific interactions, bilayer fluidity, NP-membrane model affinities and interaction kinetics. Different techniques can be associated during an experiment, providing complementary data. QCM-D is the method which presents the most advantages. There is a large choice of support surfaces, allowing complementarities with all other surface analytical methods. Frequency and dissipation changes allow qualitative and quantitative information. Temperature, medium and time parameters are completely controlled. SPR measurements are limited to a short distance (about 200 nm) from the sensor for the detection of RI changes. QCM-D is also limited to a few micrometers for viscous materials to several micrometers for rigid materials. AFM method is limited to the study of a small portion of the bilayer surface. The major drawback is the loss of membrane curvature, on the contrary to the lipid vesicle model. This model allows binding interaction, defects or ruptures but not the internalization process. These surface sensitive methods are relevant principally to investigate NP attachment to the membrane model.

Membranes models for electrical measurements

Models description

Electrical measurements, first developed to study ion channels of the cell membrane, are generally performed using a patch clamp

set up. It is also possible to record ionic flows using different biomimetic membrane models (from black lipid membrane model (BLM) to SLB). In both cases, the lipid membrane is associated to an electrical device on each side of the lipid bilayer so that it is considered as a part of an electrical circuit.[51]

Ionic fluxes can be registered using a BLM experimental setup. BLM measurements, firstly described by Mueller et al. in 1962,[52] are based on the ionic permeability of a lipid bilayer. This method is currently used to depict ionic channels function and regulation at the molecular level.[53] This very simplified electrophysiological model is now used by different research teams to study NPs membrane interactions.

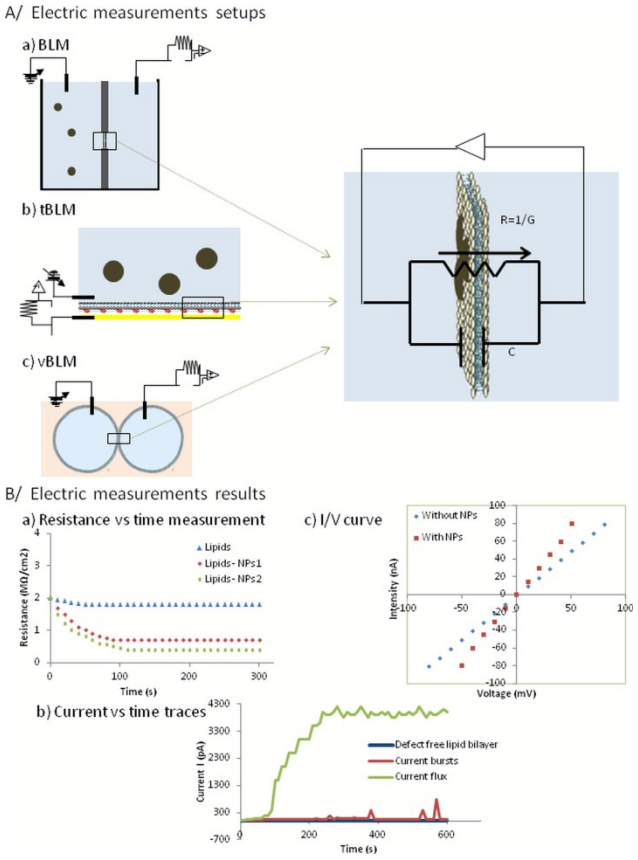

Fig. 5 : Electrical measurements are performed using three different setups: BLM, tBLM and vBLM.

A/ The different setups are: a) BLM is a lipid bilayer formed on a 150 to 200 µm diameter aperture in a Teflon plate that creates an interface between two electrolytic separated solutions. b) tBLM is a lipid bilayer supported on a conductive support such as gold and presenting an aqueous reservoir between the lipid bilayer and the solid support is present, due to the tether group. c) vBLM is obtained by water in oil vesicles. In all cases, electrodes are placed on each side of the lipid bilayer. Ensuring lipid bilayer permeability, biological membrane polarization could be mimicked. Electrical lipid bilayer properties are characterized by intensity recorded for an applied voltage. According to Ohm's law, U (V) = R (Ω). I (A), conductance G (S) = 1 / R is characteristic for the passage of ions through the lipid bilayer.

B/ Electric measurements can be expressed using the different parameters followed. Electrical changes may be monitored by a) lipid bilayer resistance; b) current-time traces; or c) intensity/voltage curves.

A BLM setup consists of lipid bilayer separating two compartments filled with an electrolytic solution in which electrodes are bathing (Fig. 5). One possible method to obtain BLM starts with dissolution of lipids in decane, this solution is "painted" in front of an aperture of 150 to 200 µm into the Teflon support. Hydrophilic lipid heads are spontaneously oriented toward the electrolytic solution and hydrophobic lipid tails with hydrophobic tails, allowing the formation of the lipid bilayer. Salt bridges connect each compartment to an electrode.

Electric measurements are also performed using the tBLM model or lipid vesicles (vBLM). The tBLM, supported on a gold sensor conductor provides a more stable model (Fig. 5Ab). The proximity to the support permits more variability for the lipid composition too.[54] On the other hand, an aqueous reservoir between the lipid bilayer and the solid support is present, due to the spacer group.[36] This reservoir allows ions exchange between *cis* and *trans* sides of the lipid bilayers. For the vBLM model, two attached water in oil droplets create two aqueous compartments at each side of the lipid bilayer. This model also leads to a more stable model than BLM (Fig. 5Ac).[55]

Methods

Without holes or ionic channels, the lipid bilayer is not permeable and ionic species cannot diffuse. Electrodes, in contact with each side of the lipid bilayer, apply a voltage in the order of mV and they show very little intensities in the pA range. Electrodes are connected to a head stage, which allows intensity amplification before recording it. This system is a tool to mimic the physiological transmembrane potential, with a negative voltage applied in *trans* compartment. Ohm's law links membrane potential (Em) to the current (intensity) and membrane resistance. Em = R.I (Em: potential (voltage) in volt (V); R: resistance in ohm (Ω); I: intensity in ampere (A)), from this, the lipid bilayer resistance is derived. In the presence of a lipid bilayer a gigaOhm (GΩ) resistance is generally observed. The conductance (G=1/R), expressed in Siemens (S), corresponds to ions crossing through the lipid bilayer. The conductance is the coefficient of a current-voltage (I-V) curve recorded through the head stage. The passage of ions from one compartment to the other is due to the presence of a pore or defect in the lipid bilayer. This method allows resistance (Fig.5Ba) or conductance variation measurements, current bursts recording (Fig.5Bb), time-dependent currents, and I-V curves (Fig.5Bc). The bilayer membrane is also a capacitance (C), where charges accumulate in regard to the surface. This capacitance can also be measured as an indicator of membrane surface area properties.

The electrical properties of the membranes could also be monitored using electrical impedance spectroscopy (EIS). A tethered lipid bilayer is modelled as an electrical circuit, where the lipid bilayer is considered as a resistance and capacitance (RC) element. The difference with the method presented above is the representation of results as Bode plots; where absolute impedance (|Z|) and phase angle (Θ) are plotted as a function of frequency. For this type of representation, the capacitor has ideally a slope of |Z |=

1 and a phase shift of Θ = 90° and the resistor has ideally a slope of |Z| = 0 and a phase shift of Θ = 0°.[56] More recently, electrical properties of membrane models have be followed using a platform enabling to monitor 32 lipid bilayers simultaneously in parallel.[57]

Main data obtained

This technique was able to detect NP membrane interactions that can be translated into electrical events. The pioneers in this field were Ramachandran et al. in 2005 that undertake the study of CdSe quantum dots (QDs) interactions with membrane using BLM.[58] Current bursts in planar lipid bilayers exposed to QDs were observed. Different CdSe QDs were compared: 2nm bare QDs, 3.2 nm polymer coated CdSe/ZnS QDs, and 5.7 nm streptavidin-conjugated core/shell QDs. The current bursts were attributed to the formation of pores into the lipid bilayer. The formation of nanopores by QDs aggregation was further confirmed by combination of electrical measurements and dye leakage assay.[59] This suggests that QDs aggregated to form nanopores allowing a flow of ionic and zwitterionic molecular species.

The nature of the NPs that form the pores could be responsible for ion selectivity depending on NP charge.[60] The electrostatic interactions of 20 nm polystyrene NPs (PNPs), coated with amidine (positive charge) and carboxyl (negative charge) groups with BLM were investigated. To this aim, different lipid bilayer compositions were tested, mixing cationic (ethylphosphocholine), zwitterionic (phosphocholine) and anionic (phosphatidic acid) headgroups. Potassium ion flow was facilitated when pores were formed following PNPs interaction with an anionic lipid bilayer. An enhanced selectivity for chloride ions was observed in the presence of pores resulting from the interaction between PNPs and a cationic lipid bilayer. This study reveals a more potent ability to disrupt the lipid bilayer with positively charged NPs, substantiating the greater toxicity of cationic NPs towards cells.[25] The same PNPs coated with amidine or carboxyl group having a diameter of 20, but also 100 nm, were studied by EIS using a tBLM model. A reduction of the membrane resistance was attributed to the presence of defects in the lipid bilayer. Using this model, the formation of pores was not directly observable due to the proximity of the solid support and the lipid bilayer. However, complementary dosage of the lipids present on the NPs after their interaction with tBLM was performed by UPLC/ESI/MS (ultra-performance liquid chromatography-electrospray tandem mass spectrometry) analysis. Cationic coated PNPs presented lipids at the surface in more important amounts than the smaller ones did. This result suggested lipid extraction from the tBLM by cationic NPs after adsorption on the bilayer.[57]

The passive penetration of different gold coated NPs was investigated by the measurement of membrane capacitance using a BLM experimental setup.[61] The spontaneous adsorption of MUS:OT coated gold NPs, with a core size comprised between 7 and 10 nm, was monitored via membrane capacitance changes that were recorded as electrical markers of the lipid bilayer properties. The results were correlated to cell tests performed using 3T3 fibroblast cells. NPs were labelled with a fluorescent dye to visualize them by confocal laser scanning microscopy and flow cytometry. The internalization of NPs was observed mainly at 37°C for NPs smaller than 10 nm. At 4°C, only some 9.1 and 9.8 nm NPs were internalized. This indicates that cell internalization was mainly associated with active mechanisms. These results correlated well with the model membrane experiment, NPs can interact with BLM only for a diameter smaller than 10 nm.

Another study compared CdSe well-known QDs and carbon nanotubes (CNTs) with 20-25 nm outer diameter, 5-10 nm inner diameter and a length of 10-30 µm on the BLM membrane model.[62] On the contrary to current bursts induced by QDs, a continuous and growing ion flux was induced after interaction of CNTs with BLM. The authors hypothesized the formation of transmembrane CNTs channels, upon irreversible insertion of CNTs through BLM, which transport ions through the lipid bilayer. This is an example of shape-specific mechanism governing the compared interaction of CNTs and QDs with the lipid bilayer.

NPs-BLM studies mainly concern NPs which have a diameter inferior to 25 nm. However, De Planque et al. compared 50 and 500 nm silica NP behaviour towards bilayers. Electric measurements performed by the vBLM model showed that both NPs were able to induce a current depending on the NPs surface charge, demonstrating a non-specific size-effect of NP interactions with lipid bilayers.[55]

The interactions of silver NPs (AgNPs) with a tBLM membrane model composed on 1,2-diphytanoyl-sn-glycero-3-phosphocholine (DiphyPC) was recently reported. The effects of NPs were followed using electrical impedance spectroscopy (EIS). The lipid bilayer was exposed to 150-300 ng of AgNPs. Despite large variations in the absolute values recorded, the membrane resistance was always decreasing, thus indicating a perturbation of the lipid bilayer. The electrical measurements have been associated to chemical analysis of AgNPs that had interacted with the lipid bilayer, using ICP-MS (inductively coupled plasma mass spectrometry analysis). Only about 9% of AgNPs had interacted with the lipid bilayer, and NPs that had adsorbed were almost completely removed after several rinsing steps, associated to reversible impedance changes.[63]

Indeed, to observe more specific interactions, lipid bilayer compositions could be changed. It was shown that QDs nanopore formation occurred in a lipid bilayer composed of negatively charged or net neutral lipids.[59] This data indicates that nanopore formation was not influenced by electrostatic repulsion. Plus, it seems that no effects were observed when DOPC was replaced by POPC/POPE mix to investigate QDs or CNTs interactions with BLM.[64] NPs-BLM experiments were always performed with lipid bilayers in the liquid phase. There was no NP adsorption into the lipid bilayer in the gel phase.[61]

Using a platform enabling to monitor 32 lipid bilayers in parallel, it was possible to investigate simultaneously, NPs effect, suspension medium effect and lipid composition of the bilayer during NPs membrane interactions. In this work, 60 nm polystyrene NPs bearing COOH or NH_2 on their surface were injected at different concentrations (from 25 to 100 µg/mL), different ionic strengths (from 5 to 150 mM NaCl, pH = 7), different pH (4.5, 7, 10) on top of

lipid bilayers. The lipid composition effect has also been explored, in terms of bilayer net surface charge (neutral, negatively or positively charged), or in the presence of serum proteins, for mimicking lysosomal or brain membranes environment. For all experiments, a periodic sweep composed of 70 mV for 23 seconds and -70 mV for 23 seconds was applied during two hours unless the lipid bilayers were ruptured earlier. The percentage of bilayer that ruptured and pore size analysis were the two main parameters used to compare all the conditions that were investigated.[57]

Advantages and drawbacks

Electric measurements performed on different bilayer experimental setups allow a comparison of the different properties of NPs influencing NPs-cell membrane interactions. These properties, such as charge[60], hydrophilic/hydrophobic ratio[61], shape[62], or size[55] are already recognized as parameters influencing NPs cell membrane interactions with *in cellulo* models. The correlation between these *in vitro* assays and *in cellulo* results shows the power of this method to investigate interactions between NPs and model membranes. Electrical measurements on different bilayer settings could be performed, parameters such as current fluctuation (in response to a potential), membrane resistance, and membrane capacitance could be recorded providing sensitive and quantitative results.

These methods can be seen as predictive assays for the study of NP toxicity effects on cells. Doses causing electrophysiological effects are relevant with the sub-toxic concentrations found with *in vitro* cell culture assays. For example, 50 µg/ml of 500 nm aminated silica NPs decreases cell viability.[65] Concentration tested using BLM was 100 fold lower, and was found to induce lipid bilayer disruption. In the case of CdSe QDs coated with a ZnS shell, a cellular cytotoxicity was noticed around 6 µM.[66] The concentrations injected during BLM experiments were 37.5 fold lower than the observed cellular cytotoxicity concentrations.[59] The relevance of electric measurements in nanotoxicology seems to concern low dose effects. A non-cytotoxic concentration of NPs can induce lipid bilayer disruption.

Concerning PNPs, cell viability assays and cytotoxicity mode of action were investigated using the same concentrations as those used in BLM experiments.[60,67] IC50 (inhibitory concentration of 50% of cell viability) of cationic coated NPs were of 40 µg/ml for 50 nm NPs and 50 µg/ml for 100 nm NPs, on rat alveolar macrophage cells (NR8383). BLM experiments showed pore formation from 50 µg/ml. On the other hand, anionic NPs didn't induce a decrease in the cell viability for doses up to 120 µg/ml. However, they can lead to the formation of ion specific pores in lipid bilayer from a concentration of 100 µg/ml.

These comparisons between NP concentrations inducing cytotoxic effect and lipid bilayer disruption must be taken with caution. Indeed, both assays are not achieved using exactly the same NPs. Moreover; cytotoxic assays are generally performed in the presence of FCS (fetal calf serum), in cell growth media which contains proteins which change the NP surface properties. For example, porous silica NPs doesn't show exactly the same porosity. On the other hand, CdSe QDs haven't the exact same size in the absence or presence of proteins. So the comparison with *in cellulo* assays might be strictly indicative. Only comparisons of NPs-BLM and cell assays performed in a same study, with comparable conditions are really relevant.[61]

Until now, reported variation of the lipid bilayer composition for the different assays was limited. DOPC is the more frequently used molecule in lipid membrane models. Nevertheless, in different studies it was compared with asolectin, 1,2-dioleoyl-sn-glycero-3-phosphate (DOPA), or DiphyPC. The BLM method is limited by the small available area of the lipid bilayer, formed on an aperture of 150 to 200 µm diameter, compared to the one hundred nanometer size range of NPs.

The major drawback is the lack of homogeneity in the expression of the electrical measurement results. They are expressed using different settings: number of events, I-V curves, membrane capacitance, etc. So, it becomes difficult to compare the data obtained in different studies because of different methodologies. Two teams, Posner and Wunder, tried to compare their methodologies and results, which gave a good qualitative but poor quantitative reproducibility. This study demonstrates that almost 5 trials are needed to get a valid result with BLM experiments.[64]

The lipid bilayer can be slightly unstable, which limits time-dependent experiments. The tBLM model is stabilized over time due to its attachment to a solid support. It results in a lack of reproducibility because very small external interferences such as electrical, electromagnetic field or liquid movements could cause large fluctuations which could lead to bilayer rupture.[53] Some teams tried to standardise this method to limit the differences between experimental results.[15] The recent work describing a platform to study 32 lipid bilayers simultaneously in parallel is a good prospect in response to all the drawbacks.[57]

Langmuir monolayers

Model description

Langmuir lipid monolayers are composed of one lipid leaflet formed at the air/liquid interface (Fig.6A). Hydrophilic lipid heads are oriented towards the liquid phase whilst hydrophobic tails face towards the air. After deposition of an organic solution of lipids at the air/liquid interface and evaporation of the solvent, a movable barrier set in the Langmuir trough permits the compression of the monolayer.

A sensor at the air-water interface allows the measurement of parameters such as lipid surface area and surface pressure recorded as pressure - area isotherms (π – A) from which lipid packing and elasticity can be derived.

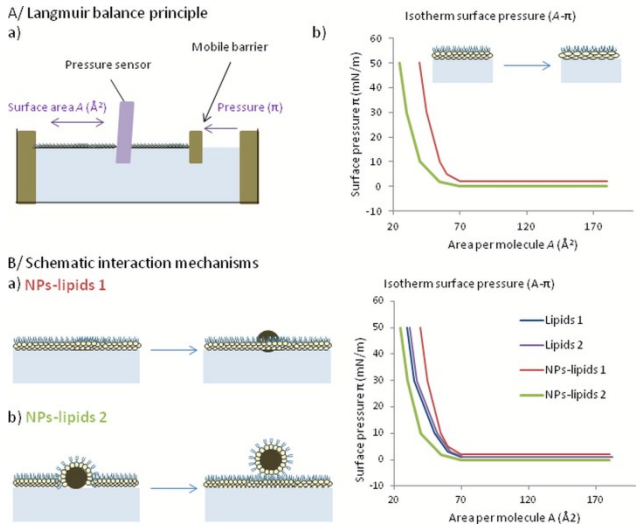

Fig. 6 : A/ Langmuir-Blodgett balance principle. a) A lipid monolayer is formed at air liquid interface between two Teflon barriers. One movable barrier induces a pressure which is measured by the sensor at the air-water interface that is inserted into the lipid monolayer. b) Lipid packing and elasticity are derived from the measurable parameters; lipid surface area and surface pressure. The phase pressure/area isotherms (π – A) are drawn to characterize the monolayer state. The Langmuir film balance is classically associated with a Brewster angle microscope to observe homogeneity of the film surface.

B/ Interaction between the lipid monolayer and NPs placed in the aqueous medium under monolayer are schematized, associated to surface-pressure isotherms. Surface pressure isotherms represent lipid monolayers (Lipids1: blue line, Lipids2: violet line), and two mechanisms are proposed for the interaction with NPs (NPs-lipids1; red line, NPs-lipids2; green line). In diagram a), NPs (NPs-lipids1; red line) spontaneously penetrate into the lipid monolayer. Lipids remain well-packed at the air-water interface, inducing an increased area per molecule per surface pressure. In diagram b) (NPs-lipids2; green line), NPs strongly interact with hydrophilic lipid head groups. Lipids surround NPs, which move from the air-water interface to the air medium. So surface pressure isotherms help to understand NPs-lipid interactions (Inspired from Uehara et al).[68]

Methods

A Langmuir balance is frequently associated to complementary methods such as Brewster angle microscopy (BAM), sum-frequency generation (SFG) vibrational spectroscopy, infra-red reflection-absorption spectrometry (IRRAS), grazing incidence X-ray diffraction (GIXD), total reflection X-ray fluorescence, and also AFM. SFG is a highly surface specific optical technique, providing information on molecular symmetry. IRRAS allows the determination of structural characteristics of lipids at the interface. GIXD and X-ray fluorescence could provide a percentage of the interfacial area occupied by NPs at different surface pressures, including the percentage of squeezed NPs. BAM and AFM indicate NP squeezing on the lipid monolayer. The combination of these different methods allows mechanistic data on NP lipid monolayer interactions to be recorded.

Main data obtained

Electrostatic interactions between NPs and lipid monolayers have been characterized from Langmuir balance experiments.[69] The interaction of anionic citrate-functionalized gold NPs (Au(Cit)-NPs) and poly(allylamine hydrochloride) cationic gold NPs (Au(PAH)-NPs) were studied with zwitterionic (dipalmitoylphosphatidylcholine (DPPC)) and anionic (dipalmitoylphosphatidylglycerol (DPPG)) lipid monolayers. Surface pressure - area isotherms for both lipid monolayer models with water, two coated-NPs concentrations, and the free coating molecule were analysed. When comparing free molecules and coated NPs, the isotherms showed that for the same surface pressure, there was an increased area per molecule, which indicated electrostatic interactions between cationic coated NPs and anionic DPPG lipid monolayers. However, counter ion effects of Na^+ cations allowed interactions between anionic coated NPs and zwitterionic DPPC lipids. Changes in the elasticity were investigated using the surface compressional modulus (Cs^{-1}), which is the measure of the in-plane elasticity of the monolayer. The surface compressional modulus were calculated from surface pressure - area isotherms via the expression $Cs^{-1}=-A\,(\partial\pi/\partial A)$, where A is the area per molecule (Å^2) and π is surface pressure (mN/m). For a real cell with a lateral pressure of 30-35 mN/m, the elasticity of the DPPG lipid monolayer was significantly affected for both anionic and cationic coated NPs, at the highest concentrations. First, Au(Cit)NP decreases DPPG elasticity, while Au(PAH)NP was found to increase it. On the other hand, only the higher concentration of Au(Cit)NP induced a significant effect on DPPC monolayer properties, with a high increase in elasticity. As expected, most effects were observed for the interactions between cationic NPs and lipid monolayers. However, effects of anionic NPs were non-negligible, in particular with zwitterionic DPPC lipids, demonstrating the significant role of counterions which are rarely considered. Significant modifications in elasticity were consistent with the cellular toxic effects related to cationic NPs.

A different scenario for cationic or anionic NPs was deduced by combination of SFG and Langmuir balance experiments.[68] DPPC and DPPG lipid monolayers were used as membrane models to interact with anionic and cationic coated NPs. Anionic NPs were dextran-coated and cationic NPs were coated with poly(diallylmethylammonium chloride) (PDAC). Due to the smaller area per lipid and SFG intensity changes, NPs seemed to remove DPPC molecules from the air-water interface. This resulted in the coverage of NPs by lipids, which caused the NPs to move above the lipid monolayer into the air. Concerning the DPPG monolayer, unlike in the previous study, no interaction was observed with anionic NPs, due to electrostatic repulsion. Cationic NPs interacted with the DPPG monolayer, inducing an increased area per molecule, but SFG intensity didn't change, indicating that lipids remained well-packed and organized at air-water interface.

Two studies were designed with a lipid monolayer composition approaching the targeted-cell membrane. The first one aims to investigate NP interactions with endothelial cells to predict NP cellular uptake.[70] To achieve this, the lipid monolayer was

composed of DPPC, DPPE, Phosphatidyl inositol (PI), (1, 2-dipalmitoyl-phosphatidylsérine) DPPS, sphingomyelin (SM), and cholesterol. These lipids were mixed according to the endothelial cell membrane composition. Langmuir balance surface pressure isotherms were combined with AFM analyses and cellular assays on human vascular endothelial cells (HUVECs). On the other hand, a comparative study about cationic NP interactions with plasma or endosomal membrane models was recently published.[71] Plasma and endosomal membrane models allowed the comprehension of NPs mechanisms involved during cellular uptake and endosomal escape. The two different surfactant-modified PVA (poly (vinyl alcohol)) NPs showed different interactions, for the same size. The zeta potential of CTAB modified PVA-NP was -14.3 mV while it was -40 mV for DMAB modified PVA-NP. Membrane lipid isotherms showed a slight shift following CTAB modified PVA NP exposure. In contrast, membrane lipid isotherms presented a different shape after DMAB modified PVA NP exposure compared to non-modified or CTAB modified NPs. DMAB modified NPs seemed to remain in the monolayer even at higher lipid densities. The authors suggested a facilitated bending of the lipid monolayer while CTAB caused bending resistance. The results highlight the endocytosis and endosomal release ability of both surfactant-modified NPs, showing the relevance of using Langmuir film monolayers to investigate these mechanisms. The observed correlation between Langmuir monolayer balance results associated to cellular uptake and cytotoxicity assays showed the complementary of the lipid monolayer model with cellular experiments.

Advantages and drawbacks

This method is useful to decipher electrostatic interactions of magnetic NPs with lipid monolayers.[68] This unsupported lipid membrane model allows particular data related to the interactions between NPs and the model membrane to be calculated. In this configuration, thermodynamic differences appear in comparison to lipid bilayers.[72] Monolayers are often in a metastable state in condensed phases. Monolayers are also less hydrated than lipid bilayers. In the case of the higher hydration state of a monolayer (liquid expanded surface phase), less water molecules are inserted between phospholipids than into the corresponding lipid bilayer in the less hydrated state (liquid crystalline phase). For a liquid expanded DPPC monolayer, the area per phospholipid molecule is measured at 53.2 $Å^2$.[73] On the other hand, a fully hydrated liquid-crystalline bilayer presents an area per phospholipid molecule of 62.9 $Å^2$.[74] Also, the dynamics between both models are also different. In most of NP-lipid monolayer interactions studies conducted at the air-liquid interface, DPPC lipids monolayers are currently used as membrane models. However, Langmuir monolayers can be formed using a large variety of lipids, saturated, unsaturated, mixed or pure and that they can be associated or not to proteins. Also, this could be an opportunity to take advantage of the diversity of Langmuir monolayers in their use as membrane models to further explored for NP-membrane interaction studies.

Modelisation methods

Model description

With the evolution of computing capacities, the computing and modelling data concerning NP-cell membrane interactions are continuously increasing. In comparison with *in vitro* results, theoretical calculations and computer simulations are able to emphasize and define precise mechanistic details concerning NPs-cell membrane interactions. Theories provide calculations in the length scale ranging from tens of nanometers to some micrometers, while molecular simulations concerning length scales from several angstroms to hundreds of nanometers.[75] These investigations provide complex information at the molecular level and in well-defined conditions.

Method description

The initiation of computational methods leads to the formulation of a mathematical model which includes numerous parameters to obtain physically relevant results. The model method is firstly defined by its force-field. The force-field describes bond stretching, bending and rotation or non-bonded interactions, such as electrostatic or van der Waals interactions.[76] The all atom force field takes account of every atom. This model is expensive and time-consuming due to the complexity of the computer calculations. Other force field methods combine several atoms and consider it as a single bead to increase the computational efficiency. For example, the united-atom force field combines aliphatic carbons and associated hydrogens in a single bead. This method is currently used to model lipid bilayers of the cell membrane.[75] However, to simulate membrane interactions with NPs in greater length scale, this explicite model is unsuitable. So implicit models using different degrees of coarse-graining were developed.[77] In the coarse-grained force field, larger molecular units are associated in a single bead. The growing interest for this force field is due in part to the possibility of using different coarse-grained degrees. With this model, lipids can be reduced to three beads, which represent one lipid molecule (Fig.7). The lipid membrane can also be represented as units corresponding to membrane patches, where details of the lipid bilayer are completely ignored, to model interaction with NPs larger than 5 nm.[77] Molecular reduction provides a better computational speed. Another strategy to enhance the computational efficiency is the use of the implicit water model. NP-cell membrane interactions are modeled either using a theory or simulation calculation. Theory consists of applying physical equations to solve a problem, whilst simulation consists of virtually reproducing the system, taking into account the physical and chemical parameters.

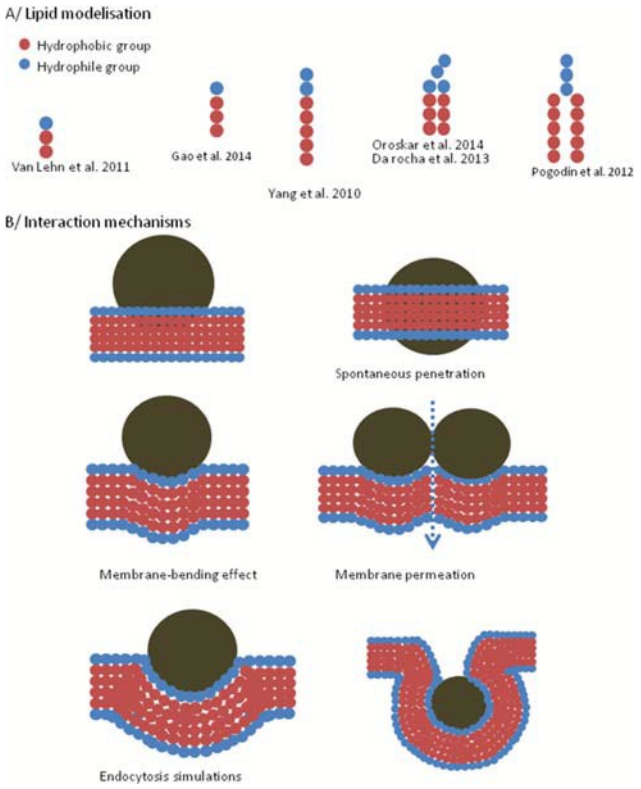

Fig. 7 : Lipid molecule modelisation. A/ Examples of lipid modelisation used for NPs-membrane model interaction studies. Lipid molecules are schematized as little beads. The more beads are used (i.e. 13 beads) the more modelisations are time-consuming, however results are more realistic. When a lipid molecule is reduced to 3 beads, calculations are faster but the results are less precise. The choice of lipid model will influence the data obtained. B/ Three major mechanisms are observed by modelisation methods for NPs-lipid bilayer interactions after NPs binding to the lipid bilayer: spontaneous penetration, membrane-bending effect, membrane permeation. NP binding to the membrane model can also lead to endocytosis-like penetration, through membrane invagination followed by vesicle formation. Several calculations record a lot of informations such as the involved energy forces.

Main data obtained

Dynamically rearranging ligands onto the NP surface, in response to the environment, is a possible assay that can be solved only using modelisation[78]. The initial NP surface was composed of hydrophilic and hydrophobic ligands arranged with two configurations: Janus or mixed configuration. The NP-bilayer system was modelled with coarse-grained simulations. An explicit solvent bilayer model conceived by Cooke et al,[79] was used where each lipid was modelled as a hydrophilic head bead associated with two hydrophobic tail beads. NPs were uniform spherical hollow shells of beads. Beads represented the hydrophilic or hydrophobic ligands at the NP surface. Two simulation algorithms were simultaneously used to study the dynamic rearrangement of ligands at the NP surface: Brownian dynamics and Monte Carlo algorithms. Brownian dynamics simulate the motion of beads in the bilayer system. Monte Carlo was used to aleatorically switch adjacent beads in order to preserve an optimal ligand arrangement. These simulations resulted in five different configurations obtained spontaneously. From the completely mixed hydrophilic and hydrophobic ligands at the NP surface, no interaction was evidenced between NPs and the lipid model. When surface ligands were rearranged, with most hydrophobic ligands in contact with lipid bilayer, a weak complexation was observed. A symmetric penetration then occurred if all hydrophobic ligands were embedded in the bilayer core and if the protruding spherical caps were hydrophilic. From the Janus configuration, asymmetric penetration was observed showing hydrophobic ligands anchored in the lipid bilayer without deformation. Some hydrophobic ligands in contact with surrounding medium induced better penetration of NPs, leading to the wrapping of the lipid bilayer around all hydrophobic ligands. Theory calculations were complementary to the coarse-grained simulation, to understand symmetric or asymmetric penetration mechanisms of NPs in the bilayer. The free energy change occurring for the two configurations was calculated, with the lower free energy state preferred at equilibrium. For theory calculations, the discretized approach used in simulation was replaced by the continuum approximation for NPs and the lipid bilayer system. Surface energy and line tension were calculated from the Ising model using a mean-field approximation. Theory showed that the key parameter governing NPs penetration was the interaction energy between neighboring ligands on the NP surface. When placed at an order-disorder transition, symmetric penetration was favored. When the interaction energy was above the order-disorder transition energy, Janus penetration was favored. This work showed the complementarities of simulation and theory to study a complex NP-lipid bilayer interaction system.[78]

Spontaneous penetration mechanisms of NPs presenting different ligands arrangements at their surfaces into lipid membranes were also performed.[80] Dissipative particle dynamic simulations gave mechanistic information, while free energy change calculations provided quantitative data. Two lipid bilayer model systems were compared: flat membranes and vesicles. Hydrophilic and hydrophobic ligands were arranged around NPs, as stripy, patchy or random NP model. NP-lipid bilayer interaction mechanisms, such as penetration, aggregation, and pore formation were evidenced. These results might have important applications in NP design. These surface effects were then extensively studied using coarse-grained simulations. Coarse-grained simulations were frequently used to compare NP characteristics on NP-lipid bilayer interaction: passive penetration, translocation, wrapping, lipid bilayer permeation. Some NPs parameters were compared, such as hydrophilic/hydrophobic ratio, surface charge, ligands length, arrangement and surface density coatings, NP shape, size, etc.

These different NP parameters were then studied with coarse-grained molecular dynamics.[81] In this case, coarse-graining was very precise, using 12 beads per lipid molecule. Two lipid bilayer models were studied; the first one composed of DPPC was characterized by neutral net charge and the second one containing a mixture of DPPC and DPPG which had a net negative charge. NPs composed of a 2.2 nm gold core were associated to a self-assembled covering alkylthiol monolayer (about 100 alkylthiols per Au core). One bead

represented either gold or sulfur atoms and 5 beads were used for each alkyl chain. Six different configurations were obtained, anionic, cationic, and hydrophobic NPs in contact with a neutral or negative lipid bilayer model. Cationic NPs spontaneously interact with both neutral and negatively charged lipid bilayers. Anionic NPs interact with a neutral lipid bilayer. The interactions between hydrophobic NPs and the lipid bilayer were not spontaneously favored. Interactions were more favorable between cationic NPs and negative lipid bilayers. An effect on the surface charge density was observed, when comparing the different cationic coatings (0, 20, 40, 60, 80, and 100 %). With a 20 % cationic coating, NPs were inserted into the lipid bilayer and they stayed stably embedded in the hydrophobic core. With 100% cationic coating, wrapping was observed. Occurrence of lipid bilayer disruption decreased with a growing surface charge density.

Another study using the bond fluctuation method and Monte Carlo simulations focused on NP-lipid bilayer interactions whilst varying the different hydrophilic/hydrophobic ratios at the NP surface.[82] The NPs and the lipid bilayer were modelled by coarse-grained simulation, represented by a lipid molecule using 13 beads (three head beads and ten tail beads) and NPs using 4 beads. Solvent molecules were represented by one bead. NPs were modelled with a diameter similar to the thickness of the phospholipid membrane. NPs with four different hydrophobic/hydrophilic characteristics were studied. Hydrophilic NPs didn't translocate and induced negligible permeability of lipid bilayer. Hydrophobic NPs formed aggregates which were embedded in the lipid bilayer core, which also didn't translocate. In the case of amphiphilic NPs, there was no aggregation and the NPs translocated through the lipid bilayer, inducing membrane permeability for solvent molecules and reversible disturbance of the membrane.

Membrane permeation was more precisely described in another simulation study.[83] This work used a coarse-grained model of DPPC lipid bilayer membranes and a MARTINI force field. 2 or 3 nm diameter NPs functionalized with small or long butane-thiol ligands were studied. These hydrophobic ligands interacted with lipid tails, inducing lipid loss. Interaction between NPs and the lipid bilayer was then followed by a water permeation event leading to lipid "flip-flop" and ion penetration. The pore-mediated permeation of the lipid bilayer, associated with a "water finger", was fully described. It was also shown that chloride ions were more suitable to flow through the lipid bilayer than sodium. These results were consistent and related to electrophysiological studies,[60] and could be extended to other NPs.

The effects of NP shape and volume for the translocation process were studied both with dissipative particle dynamics[84] and the coarse-grained simulation model.[85] Both studies compared NPs with a maximum length of 4 nm which have anionic, neutral and cationic surfaces. The first study compared the interaction of ellipsoidal, cylindrical or pushpin-shaped particles with a lipid bilayer.[84] Data derived from the driving force applied to the center of the particle in the z-direction induced NP penetration through the lipid bilayer. Results obtained with dissipative particle dynamics showed the important effect of particle shape anisotropy and the initial orientation of the particle. These data were confirmed with coarse-grained molecular dynamics.[85] In this work, sphere, pyramid, rice, cone, rod and cube shaped NPs were considered. Quantitative data were obtained from free-energy activation barrier values for a constant force applied in the z-direction, from which rate constants and half-lives of NPs translocation were calculated. If the penetration of NPs in the bilayer seemed to be more difficult when the contact area was at a maximum,[84] penetration was facilitated by planar surfaces.[85] So pyramidal NPs translocated more easily than conical NPs, and faceted rice NPs penetrated more easily than rod like NPs. Then, the effect of shape on endocytosis kinetics was studied with dissipative particle dynamics.[86] Coarse-grained simulations were used to model DMPC lipids and NPs with sphere, rod, and disk shapes. This endocytosis mechanism simulation model considered membrane receptor-NP interaction. Results showed that endocytosis happened the fastest for sphere->rod->disk-shaped NPs. Endocytosis of NPs with shape anisotropy was associated with a rotation leading to a maximum contact area between NPs and the lipid bilayer, leading to membrane wrapping. NPs with shape anisotropy often induced asymmetry during the internalization pathway, due to an important membrane tension associated to the wrapping stage.

Endocytosis simulations were performed to study NP size effect during endocytosis phenomena. While most simulation studies were performed with NPs smaller than 5 nm, NP size effect has already been experimentally demonstrated. A dissipative particle dynamics simulation on interaction between the lipid bilayer (DPPC) and 6.25, 12.5, 25 and 37.5 nm hydrophilic spherical NPs was realized.[87] Two different wrapping modes were described: membrane bending-controlled mode obtained for weak membrane-NP adhesion and lipid diffusion dominated mode, for strong membrane-NP adhesion. The relationships between endocytosis rate and NP size were evidenced by simulation. A large contact area between NP and lipid bilayer promotes wrapping. So, NP wrapping was controlled by the balance between membrane-NP adhesion and membrane bending energy. So larger NPs present the highest contact areas which promote membrane adhesion, so wrapping dynamics occur by the bending-controlled mode. Inversely, smaller NPs induced membrane protrusion by lipid diffusion, so wrapping dynamics were controlled by the lipid diffusion dominated mode. Finally, endocytosis process occurred faster for smaller NPs than larger ones.

Membrane-bending effects were also studied by simulations and confirmed experimentally;[49] 2 nm gold NPs were grafted using a binary mixture of alkanethiol ligands, MUS and MUS: OT. These NPs were used as reference to compare different NP-lipid bilayer interaction methods. Simulation was performed with atomistic models, using GROMMOS[88] and CHARMM[89] force fields. This atomistic method provided unbiased simulation, in which only physicochemical forces were involved. It was shown that protrusion of lipid tails into the solvent promoted the interaction of hydrophobic ligands grafted on NPs. So NPs didn't interact with

planar lipid bilayer surfaces. These data were confirmed with QCM-D and AFM experiments on SLB models.

Of notice, membrane wrapping around NPs is not only dependent on global parameters such as particle size or aspect ratio.[90] Cube-like and rod-like NPs with a size of 20-100 nm were compared through numerical calculations of deformation energy of the membrane model leading to phase diagrams. Adhesion strengths have been calculated with varying the orientation of NPs, and three different bound states have been described in this study, the "shallow-wrapped" state, the "deep-wrapped" state, and the "complete-wrapped" state. Different favorable orientations of NPs have been described for the both NPs' shapes. Also, the local geometrical characteristics of the NPs were found to play a key role in the wrapping behavior of bilayers towards NPs. On another hand, the adhesive properties of the NPs towards membranes were also found to be dependent on the local membrane curvature.[91] It's interesting to see in parallel the effect of the local geometry of the NPs and the membrane curvature. In this work, the membrane curvature was taken in account for the calculations of bending energy density and the adhesive energy of NPs to membranes. As a consequence, different membrane segments behaviors and distinct engulfment patterns were evidenced, were NPs can be free, partially engulfed, completely engulfed or in a bistable state. This introduced the principle of membrane-mediated NPs interaction. Different membrane deformations have been observed depending on NPs size, shape and surface. The local properties of the membrane were found to influence the local interaction of NPs with membranes. The understanding of NPs cell membrane interactions was not the only goal, NPs were seen as tools to control the membrane local properties. These data were of use to control the local deformation of the membrane and then obtain different structural objects from the membrane studied.[77] As an example, the formation of tubes starting from a GUV model have been simulated using large colloidal particles. [92]

Advantages and drawbacks

Computational methods offer a fast confirmation of experimental results associated with more precise data.[78] Interpretation of experimental observations is done by free energy change calculations, line tension, radial distribution functions, etc. Some assays could only be performed by simulation or theoretically, in particular for NPs with dynamically rearranging ligands on their surface,[78] special ligand arrangements[80] and controlled geometric shapes.[84, 85] Mechanistic data concerning NP-lipid membrane interactions are accessible from simulation experiments. All parameters of the system, lipid composition, charge, nanoparticle size, number, surface chemistry, medium composition, etc, are controlled.

But, the choice of the model used to simulate NPs cell membrane interactions is a critical point. A unique model can be used to study NPs with a size in the same range as the lipid bilayer thickness. However, when NPs are significantly larger than the lipid bilayer thickness, it is not possible to use only one model. Computational study requires a very good design before analysis to spare some biased results. Comparison of results obtained with different coarse graining levels is still lacking. One publication at the nano-bio interface reports simulation using atomistic models.[49] This time and cost consuming method is the only one to observe unbiased structural, chemical and physical details. Sometimes, discrepancies appear due to the use of different coarse-graining levels and simulations methods between studies. So it is very interesting to directly combine computational methods and experimental data using the same nano-bio interface system.

Conclusions

Membrane models and associated techniques

Visualization of NP-membrane interactions could be achieved using confocal microscopy, electron microscopy[30] or AFM.[47] CryoTEM is the more powerful technique to follow the progress of NPs after being in contact with membranes.[23] Microscopic observations could be performed with almost all experimental membrane models. With membrane models, interaction mechanisms could be evidenced (Fig. 7): membrane attachment, membrane disruption, or lipid properties changes. Membrane attachment is mainly characterized using the SLB model. Numerous SLB models are now available to mimic the cell membrane of interest.[36] SLB models are generally associated to surface sensitive methods: SPR, QCM-D and AFM. These methods provide monitoring of quantitative and qualitative data. Membrane disruption after exposure to NPs is characterized by vesicle leakage assay or electric measurements. Vesicles have contributed to the study of toxicological mechanisms and for understanding of numerous xenobiotic molecules before being used with NPs.[19] So, there is consistent knowledge for interpretation of such results that will be obtained with NPs. On the other hand, electrical measurements, classically used to study ion channels, are also used to evidenced membrane disruption.[64] The electrical measurements of NPs-lipid membranes interactions have been performed using the lipid vesicle model, SLB or an unsupported planar lipid bilayer. Changes to the lipid properties such as membrane thickness, fluidity, lateral lipid mobility and lipid diffusion coefficients could be characterized using FRAP or Langmuir monolayers, for example. Theoretical and computational investigations are consistent with experimental models concerning the influence of NP's physicochemical properties on NP-membrane interactions.[75] Plus, these models are useful to investigate the impact of NP surface ligands (ligand length, density, position, hydrophobicity/hydrophilicity) on the interaction with cell membrane. It is also possible to determine the force energy involved during NP-membrane interactions.

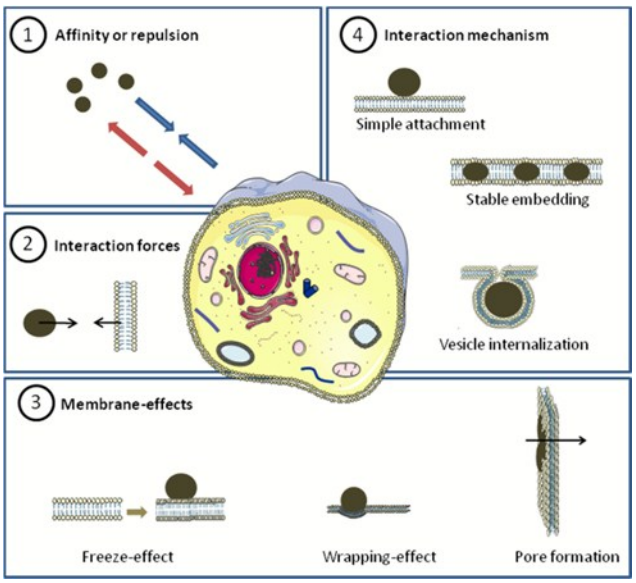

Fig. 8 : NP-cell membrane interactions studied using membrane models. The NP-cell membrane interaction mechanism could be divided in 4 steps: 1) Affinity or repulsion, depending on NP surface properties (charge, ligands, protein corona). This step could be characterized using surface sensitive methods using the SLB model. 2) Interaction forces between NPs and the cell membrane are also dependent on NP surface properties. They could be determined using modelisation models. 3) Membrane-effects, such as the freezing-effect, wrapping-effect and pore formation could explain some cellular toxic effects. The freezing-effect demonstration could be obtained by using FRAP, DSC, or Laurdan assay experiments. FRAP and/or microscopic observations could visualize the wrapping-effect. Pore formation has been monitored by performing electric measurements, dye leakage assays and AFM studies. 4) The resulting NP-membrane interactions could be simple attachment to the membrane, or stable embedding of NPs into the lipid bilayer or internalization via vesicles.

Interaction mechanisms

Membrane models are currently used to understand the influence of the physicochemical properties of NPs on their interactions with membranes. Protein corona composition, NP size, shape, charge, hydrophilicity/hydrophobicity ratio, ligand length, density or surface repartitions were particularly investigated. The impact on 4 different steps has been evidenced (Fig. 7): NP affinity for the membrane model, NPs binding to the membrane, the effect of NPs on physical state of the lipid membrane and the resulting interaction between NPs and the cell membrane. Firstly, NPs affinity for the membrane model is mainly influenced by the NP's charge, corona composition, or hydrophilicity/hydrophobicity ratio. Positively charged NPs are attracted by the negatively charged cell membrane (Fig. 7-1). Corona proteins recognized by cell receptors promote NP-cell membrane interactions. Hydrophobic ligands that are present at the NP's surface could insert through the lipid bilayer. This has been shown using the GUV model[30], BLM[60], Langmuir-Blodgett film[69], SLB/SPR[44] and was confirmed by computational methods.[81] NP affinity is followed by the second step, in which NPs bind to the membrane (Fig. 7-2). NP-membrane interactions could involve Van der Waals or electrostatic forces, or ligand insertion into the lipid bilayer. These interactions forces could be calculated by modelisation models [78,75] and depend mainly on the NP charge, ligand properties, and the surface ligand hydrophilic/hydrophobic ratio. Step 3 concerns the effect of NPs on the physical state of the lipid membrane (Fig. 7-3). Membrane effects, which include the freeze-effect, the wrapping-effect or pore formation, are also dependent on NP size and shape. Concerning NP shape, the NPs present in the larger planar surface could interact better with the lipid bilayer. So, irregular surfaces or small particles radii lead to few interactions with the lipid bilayer. The smaller NPs from 1.2 to 20 nm, with high affinity for the lipid membrane (cationic or hydrophobic surface) promote pore formation. Pore formation is classically characterized using dye leakage assay[19] and electrical measurements,[64] but could also be observed with AFM[45] and simulation experiments.[83] NPs in the range of 20 - 50 nm could interact with the lipid bilayer, but not directly penetrate it. This generally induces a freeze-effect that has been observed using Laurdan assay[31, 93], DSC[33], and FRAP experiments.[22] Larger NPs, with a diameter of 50 to 200 nm, are able to deform the lipid bilayer inducing a wrapping effect. This wrapping-effect has been evidenced by FRAP, microscopy[22], and confirmed by modelisation experiments.[94] Finally, all NP properties influence the resulting interaction between NPs and cell membranes (Fig. 7-4). Simple attachment to the membrane could be easily monitored by SLB using surface sensitive methods such as QCM-D.[48] Stable embedding, following the freeze-effect, has been deduced from FRAP results[22] and confirmed by simulations.[82] Vesicle internalization, generally following the wrapping-effect, is observed by cryoTEM[23] and more data could be recorded thanks to simulations.[87] Lipid membrane models allowed the three first steps to be evidenced whilst the fourth could also be obtained by cellular experiments. The third step, however, could explain some toxic effects. The membrane-effects induce a loss of membrane functionality. Membrane proteins and molecular transportation are possible when the lipid membrane is in a fluid phase. Freeze-effect results in an increased membrane rigidity, which is then able to disturb cellular signaling and trafficking.[95] In the same way, pore formation induces ions passage through non regulated channels. Ion equilibrium perturbation is responsible for toxic effects.

Membrane models and NPs-cell interactions

Membrane models are useful platforms for the investigation of NP-cell membrane interactions in controlled conditions. Medium composition (salts, pH, proteins…), lipid membrane composition (phospholipids, cholesterol, and membrane proteins), and physical conditions (light or temperature exposure) are controlled. The choice of lipid composition is a critical point for the study of NP interaction with model membranes. It is worth noting that membrane models don't provide a toxicity assessment but instead a mechanistic input on toxic effects associated with membranous lipids. But membrane models provide precious data on steps occurring from the exposure of membranous lipids to the process of NP-membrane interaction. The details directly related to lipid properties, only accessible by membrane models, are crucial to

assess the NP's toxic potential. As an example, the difference in the internalization pathways and toxicity for smaller (1-20 nm and 20-50 nm ranges) and bigger (50-200 nm) NPs are clearer.[12] Smaller NPs show slight membrane penetration but induce an important toxicity. This can be explained by hole or pore formation in the lipid bilayer, leading to a loss of membrane functionality. On the contrary, bigger NPs are easily internalized into vesicles, but it results in a low toxicity effect. This suggests the existence of a critical particle radius, or an optimal NP size to induce maximum disruption or the endocytosis penetration mechanism.[12]

Abbreviations

AFM	Atomic force microscopy
AgNPs	Silver NPs
ApoE-Ab	Anti-apolipoprotein E antibody
Au(Cit)-NPs	Citrate-functionalized gold NPs
Au(PAH)-NPs	Poly (allylamine hydrochloride) gold NPs
AuNPs	Gold NPs
BLM	Black lipid membrane
BSA	Bovine serum albumin
CNTs	Carbon nanotubes
DAD	Diallyldiammonium
DiphyPC	1,2-diphytanoyl-sn-glycero-3-phosphocholine
DLVO	Derjaguin-Landau-Verwey-Overbeek
DMPC	1,2-dimyristoyl-*sn*-glycero-3-phosphocholine
DMPAC	Dimyrylstoylphosphatidic acid
DMTAP	1,2-dimyristoyl-3-trimethyl-ammonium-propane
DNA	Desoxyribo nucleic acid
DLPC	1,2-dilauroyl-sn-glycero-3-phosphocholine
DOPA	1,2-dioleoyl-sn-glycero-3-phosphate
DOPC	1, 2-dioleoyl-phosphatidylcholine
DOPG	1, 2-dioleoyl-phosphoglycerol
DPPC	1, 2-dipalmitoyl-phosphatidylcholine
DPPG	1, 2-dipalmitoyl-phosphatidylglycerol
DPPS	1, 2-dipalmitoyl-phosphatidylsérine
DSC	Differential scanning calorimetry
EIS	Electrical impedance spectroscopy
FRET	Förster resonance energy transfer
GIXD	Grazing incidence X-ray diffraction
GUV	Giant unilamellar vesicle
GM1	Monosialoganglioside
HAS-Ab	Anti-human albumin antibody
HUVECs	Human vascular endothelial cells
IC50	Inhibitory concentration of 50% of cell viability
ICP-MS	inductively coupled plasma mass spectrometry
IF	Fluorescence intensity
IRRAS	infra red reflection-absorption spectrometry
iSCAT	interferometric scattering microscopy
ITC	isothermal titration calorimetry
Laurdan	6-lauryl-2-(N, dimethylamino) naphtalene
LB	Langmuir-Blodgett
LRP-1	receptor-related protein-1
LS	Langmuir-Schaefer
LUV	large unilamellar vesicle
MUS	11-mercapto-1-undecanesulfonate
NPs	nanoparticles
OT	1-octanethiol
PC	phosphatidylcholine
PDAC	poly (diallylmethylammonium chloride)
PI	phosphatidyl inositol
PNPs	polystyrene NPs
QCM-D	quartz crystal microbalance with dissipation monitoring
QDs	quantum dots
RBCs	red blood cells
RI	refractive index
ROS	reactive oxygen species
SFG	sum-frequency generation

SLB	supported lipid bilayer
SM	sphingomyelin
SOPC	L-α-stearoyl-oleoyl-phosphatidylcholine
SOPS	L-α-stearoyl-oleoyl-phosphatidylsérine
SPR	surface plasmon resonance
SPT	single-particle tracking
SUV	small unilamellar vesicle
TEM	transmission electron microscopy
TiO_2 NPs	titanium oxide nanoparticles
Tm	transition temperature of melting
UPLC/ESI/MS	ultra-performance liquid chromatography-electrospray tandem mass spectrometry

Acknowledgements

We acknowledge CNRS and the National Agency of Research (ANR-13-NANO-0007-01) for financial support. We are grateful to Ellie Barlows Myers for correcting the manuscript.

References

1. EC, *Journal*, 2011, L275/ 238-240.
2. G. Oberdorster, A. Maynard, K. Donaldson, V. Castranova, J. Fitzpatrick, K. Ausman, J. Carter, B. Karn, W. Kreyling, D. Lai, S. Olin, N. Monteiro-Riviere, D. Warheit and H. Yang, *Part Fibre Toxicol*, 2005, **2**, 1-35.
3. M. De, P. S. Ghosh and V. M. Rotello, *Adv. Mater.*, 2008, **20**, 4225-4241.
4. Leem, Nanotechnologies applied to Medicine, (http://www.ariis.fr/2014/02/25/mise-a-jour-de-letude-nanotechnologies-du-comite-biotechnologies-du-leem/?from=search&pagenb=1&query=leem).
5. AFNOR, *Journal*, 2012, **FD ISO/TR 13014**, 1-33.
6. A. E. Nel, L. Madler, D. Velegol, T. Xia, E. M. Hoek, P. Somasundaran, F. Klaessig, V. Castranova and M. Thompson, *Nat Mater*, 2009, **8**, 543-557.
7. I. Lynch, T. Cedervall, M. Lundqvist, C. Cabaleiro-Lago, S. Linse and K. A. Dawson, *Adv Colloid Interface Sci*, 2007, 167-174.
8. K. Luyts, D. Napierska, B. Nemery and P. H. Hoet, *Environ Sci Process Impacts*, 2013, **15**, 23-38.
9. M. Lundqvist, J. Stigler, G. Elia, I. Lynch, T. Cedervall and K. A. Dawson, *Proc Natl Acad Sci U S A*, 2008, **105**, 14265-14270.
10. L. A. Lane, X. Qian, A. M. Smith and S. Nie, *Annu Rev Phys Chem*, 2015, **66**, 521-547.
11. B. M. Rothen-Rutishauser, S. Schurch, B. Haenni, N. Kapp and P. Gehr, *Environ Sci Technol*, 2006, **40**, 4353-4359.
12. C. M. Beddoes, C. P. Case and W. H. Briscoe, *Adv Colloid Interface Sci*, 2015, **218**, 48-68.
13. G. Sahay, D. Y. Alakhova and A. V. Kabanov, *J Control Release*, 2010, **145**, 182-195.
14. N. Lewinski, V. Colvin and R. Drezek, *Small*, 2008, **4**, 26-49.
15. K. L. Chen and G. D. Bothun, *Environ Sci Technol*, 2013, **48**, 873-880.
16. P. L. Yeagle, in *The structure of biological membranes*, ed. C. Press, Taylor and Francis Group, Boca Raton, 3 edn., 2011, ch. 3, pp. 43-66.
17. W. Stoeckenius and D. M. Engelman, *J Cell Biol*, 1969, **42**, 613-646.
18. Y. Roiter, M. Ornatska, A. R. Rammohan, J. Balakrishnan, D. R. Heine and S. Minko, *Langmuir*, 2009, **25**, 6287-6299.
19. H. H. Zepik, P. Walde, E. L. Kostoryz, J. Code and D. M. Yourtee, *Crit Rev Toxicol*, 2008, **38**, 1-11.
20. S. Bibi, R. Kaur, M. Henriksen-Lacey, S. E. McNeil, J. Wilkhu, E. Lattmann, D. Christensen, A. R. Mohammed and Y. Perrie, *Int J Pharm*, 2011, **417**, 138-150.
21. F. G. Strobl, F. Seitz, C. Westerhausen, A. Reller, A. A. Torrano, C. Brauchle, A. Wixforth and M. F. Schneider, *Beilstein J Nanotechnol*, 2014, **5**, 2468-2478.
22. S. Zhang, A. Nelson and P. A. Beales, *Langmuir*, 2012, **28**, 12831-12837.
23. O. Le Bihan, P. Bonnafous, L. Marak, T. Bickel, S. Trepout, S. Mornet, F. De Haas, H. Talbot, J. C. Taveau and O. Lambert, *J Struct Biol*, 2009, **168**, 419-425.
24. J. N. Weinstein, S. Yoshikami, P. Henkart, R. Blumenthal and W. A. Hagins, *Science*, 1977, **195**, 489-492.
25. C. M. Goodman, C. D. McCusker, T. Yilmaz and V. M. Rotello, *Bioconjug Chem*, 2004, **15**, 897-900.
26. H. Deschout, K. Raemdonck, J. Demeester, S. C. De Smedt and K. Braeckmans, *Pharm Res*, 2014, **31**, 255-270.
27. A. Celli and E. Gratton, *Biochim Biophys Acta*, 2010, **1798**, 1368-1376.
28. B. Y. Moghadam, W. C. Hou, C. Corredor, P. Westerhoff and J. D. Posner, *Langmuir*, 2012, **28**, 16318-16326.
29. H. Pera, T. M. Nolte, F. A. Leermakers and J. M. Kleijn, *Langmuir*, 2014, **30**, 14581-14590.
30. M. Laurencin, T. Georgelin, B. Malezieux, J. M. Siaugue and C. Menager, *Langmuir*, 2010, **26**, 16025-16030.
31. A. H. Churchman, R. Wallace, S. J. Milne, A. P. Brown, R. Brydson and P. A. Beales, *Chem Commun (Camb)*, 2013, **49**, 4172-4174.
32. B. Wang, L. Zhang, S. C. Bae and S. Granick, *Proc Natl Acad Sci U S A*, 2008, **105**, 18171-18175.
33. S. Ahmed, S. Savarala, Y. Chen, G. Bothun and S. L. Wunder, *Small*, 2012, **8**, 1740-1751.
34. O. L. Katsamenis, N. Bouropoulos and D. G. Fatouros, *J Biomed Nanotechnol*, 2009, **5**, 416-420.

35. C. Rossi and J. Chopineau, *Eur Biophys J*, 2007, **36**, 955-965.
36. S. Rebaud, O. Maniti and A. P. Girard-Egrot, *Biochimie*, 2014, **107** 135-142.
37. K. El Kirat, S. Morandat and Y. F. Dufrene, *Biochim Biophys Acta*, 2010, **1798**, 750-765.
38. R. P. Richter, R. Berat and A. R. Brisson, *Langmuir*, 2006, **22**, 3497-3505.
39. B. Liedberg, C. Nylander and I. Lundstrom, *Sensors and actuators*, 1983, **4**, 299-304.
40. F. Giess, M. G. Friedrich, J. Heberle, R. L. Naumann and W. Knoll, *Biophys J*, 2004, **87**, 3213-3220.
41. F. Hook and B. Kasemo, in *Piezoelectric sensors*, eds. A. Janshoff and C. Steinem, Springer, Berlin Heidelberg, 2007, vol. 5, ch. 3, pp. 425-447.
42. K. L. Hartman, S. Kim, K. Kim and J.-M. Nam, *Nanoscale*, 2015, **7**, 66-76.
43. C. L. Hsieh, S. Spindler, J. Ehrig and V. Sandoghdar, *J Phys Chem B*, 2014, **118**, 1545-1554.
44. M. Canovi, J. Lucchetti, M. Stravalaci, F. Re, D. Moscatelli, P. Bigini, M. Salmona and M. Gobbi, *Sensors (Basel)*, 2012, **12**, 16420-16432.
45. P. R. Leroueil, S. A. Berry, K. Duthie, G. Han, V. M. Rotello, D. Q. McNerny, J. R. Baker, Jr., B. G. Orr and M. M. Holl, *Nano Lett*, 2008, **8**, 420-424.
46. T. A. Spurlin and A. A. Gewirth, *Nano Lett*, 2007, **7**, 531-535.
47. Y. Roiter, M. Ornatska, A. R. Rammohan, J. Balakrishnan, D. R. Heine and S. Minko, *Nano Lett*, 2008, **8**, 941-944.
48. R. Frost, G. E. Jonsson, D. Chakarov, S. Svedhem and B. Kasemo, *Nano Lett*, 2013, **12**, 3356-3362.
49. R. C. Van Lehn, M. Ricci, P. H. Silva, P. Andreozzi, J. Reguera, K. Voitchovsky, F. Stellacci and A. Alexander-Katz, *Nat Commun*, 2014, **5**, 4482.
50. P. Yi and K. L. Chen, *Environ Sci Technol*, 2013, **47**, 5711-5719.
51. B. Hille, in *Ionic channels in excitable membranes*, Sinauer associates, Sunderland, 3 edn., 1991, ch. 1, pp. 1-21.
52. P. Mueller, D. O. Rudin, H. T. Tien and W. C. Wescott, *Nature*, 1962, **194**, 979-980.
53. M. Winterhalter, *Current opinion in colloid and interface science*, 2000, **5**, 250-255.
54. Y. Liu, Z. Zhang, Q. Zhang, G. L. Baker and R. M. Worden, *Biochim Biophys Acta*, 2014, **1838**, 429-437.
55. M. R. De Planque, S. Aghdaei, T. Roose and H. Morgan, *ACS Nano*, 2011, **5**, 3599-3606.
56. I. K. Vockenroth, C. Rossi, M. R. Shah and I. Köper, *Biointerphases*, 2009, **4**, 19-26.
57. B. Lu, T. Smith and J. J. Schmidt, *Nanoscale*, 2015, **7**, 7858-7866.
58. S. Ramachandran, N. E. Merrill, R. H. Blick and D. W. van der Weide, *Biosens Bioelectron*, 2005, **20**, 2173-2176.
59. S. A. Klein, S. J. Wilk, T. J. Thornton and J. D. Posner, *Journal of physics*, 2008, **109**, 1-4.
60. A. Negoda, K. J. Kim, E. D. Crandall and R. M. Worden, *Biochim Biophys Acta*, 2013, **1828**, 2215-2222.
61. R. P. Carney, Y. Astier, T. M. Carney, K. Voitchovsky, P. H. Jacob Silva and F. Stellacci, *ACS Nano*, 2013, **7**, 932-942.
62. C. Corredor, W.-C. Hou, S. A. Klein, B. Y. Moghadam, M. Goryll, K. Doudrick, P. Westerhoff and J. D. Posner, *Carbon*, 2013, **60**, 67-75.
63. R. V. Goreham, V. C. Thompson, Y. Samura, C. T. Gibson, J. G. Shapter and I. Koper, *Langmuir*, 2015, **31**, 5868-5874.
64. A. Negoda, Y. Liu, W. C. Hou, C. Corredor, B. Y. Moghadam, C. Musolff, L. Li, W. Walker, P. Westerhoff, A. J. Mason, P. Duxburry, J. D. Posner and R. M. Worden, *Int. j. biomedical nanoscience and nanotechnology*, 2013, **3**, 52-83.
65. Z. Tao, B. B. Toms, J. Goodisman and T. Asefa, *Chem Res Toxicol*, 2009, **22**, 1869-1880.
66. C. Kirchner, T. Liedl, S. Kudera, T. Pellegrino, A. Munoz Javier, H. E. Gaub, S. Stolzle, N. Fertig and W. J. Parak, *Nano Lett*, 2005, **5**, 331-338.
67. S. Bhattacharjee, D. Ershov, M. A. Islam, A. M. Kämpfer, K. A. Maslowska, J. v. d. Gucht, G. M. Alink, A. T. M. Marcelis, H. Zuilhofa and I. M. C. M. Rietjens, *RSC advances*, 2014, 19321-19330.
68. T. M. Uehara, V. S. Marangoni, N. Pasquale, P. B. Miranda, K. B. Lee and V. Zucolotto, *ACS Appl Mater Interfaces*, 2013, **5**, 13063-13068.
69. A. A. Torrano, A. S. Pereira, O. N. Oliveira, Jr. and A. Barros-Timmons, *Colloids Surf B Biointerfaces*, 2013, **108**, 120-126.
70. C. Peetla, K. S. Rao and V. Labhasetwar, *Mol Pharm*, 2009, **6**, 1311-1320.

71. C. Peetla, S. Jin, J. Weimer, A. Elegbede and V. Labhasetwar, *Langmuir*, 2014, **30**, 7522-7532.
72. C. Stefaniu, G. Brezesinski and H. Mohwald, *Adv Colloid Interface Sci*, 2014, **208**, 197-213.
73. H. M. Mansour and G. Zografi, *Langmuir*, 2007, **23**, 3809-3819.
74. J. F. Nagle, R. Zhang, S. Tristram-Nagle, W. Sun, H. I. Petrache and R. M. Suter, *Biophys J*, 1996, **70**, 1419-1431.
75. H. M. Ding and Y. Q. Ma, *Small*, 2015, **11**, 1055-1071.
76. A. J. Makarucha, N. Todorova and I. Yarovsky, *Eur Biophys J*, 2011, **40**, 103-115.
77. A. Saric and A. Cacciuto, *Soft Matter*, 2013, **9**, 6677-6695.
78. R. C. Van Lehn and A. Alexander-Katz, *Soft Matter*, 2011, **7**, 11392-11404.
79. I. R. Cooke, K. Kremer and M. Deserno, *Phys Rev E Stat Nonlin Soft Matter Phys*, 2005, **72**, 011506.
80. Y. Li, X. Zhang and D. Cao, *Soft Matter*, 2014, **10**, 6844-6856.
81. E. L. Da Rocha, G. F. Caramori and C. R. Rambo, *Phys Chem Chem Phys*, 2013, **15**, 2282-2290.
82. S. Pogodin, M. Werner, J. U. Sommer and V. A. Baulin, *ACS Nano*, 2012, **6**, 10555-10561.
83. P. A. Oroskar, C. J. Jameson and S. Murad, *Langmuir*, 2014, **31**, 1074-1085.
84. K. Yang and Y. Q. Ma, *Nat Nanotechnol*, 2010, **5**, 579-583.
85. S. Nangia and R. Sureshkumar, *Langmuir*, 2012, **28**, 17666-17671.
86. Y. Li, T. Yue, K. Yang and X. Zhang, *Biomaterials*, 2012, **33**, 4965-4973.
87. X. Gao, J. Dong and X. Zhang, *Molecular Simulation*, 2014, 1-7.
88. W. F. v. Gunsteren and H. J. C. Berendsen, *GROMMOS*, BIOMOS, Zürich, 54/A7 edn., 1976.
89. B. R. Brooks, C. L. B. III, A. D. M. Jr, L. Nilsson, R. J. Petrella, B. Roux, Y. Won, G. Archontis, C. Bartels, S. Boresch, A. Caflisch, L. Caves, Q. Cui, A. R. Dinner, M. Feig, S. Fischer, J. Gao, M. Hodoscek, W. Im, K. Kuczera, T. Lazaridis, J. Ma, V. Ovchinnikov, E. Paci, R. W. Pastor, C. B. Post, J. Z. Pu, M. Schaefer, B. Tidor, R. M. Venable, H. L. Woodcock, X. Wu, W. Yang, D. M. York and M. Karplus, *Journal of Computational Chemistry*, 2009, **30**, 1545-1614.
90. S. Dasgupta, T. Auth and G. Gompper, *Nano Lett*, 2014, **14**, 687-693.
91. J. Agudo-Canalejo and R. Lipowsky, *Nano Lett*, 2015, **15**, 7168-7173.
92. A. Saric and A. Cacciuto, *Phys Rev Lett*, 2012, **109**, 188101.
93. X. Wei, W. Jiang, J. Yu, L. Ding, J. Hu and G. Jiang, *J Hazard Mater*, 2015, **287**, 217-224.
94. A. H. Bahrami, M. Raatz, J. Agudo-Canalejo, R. Michel, E. M. Curtis, C. K. Hall, M. Gradzielski, R. Lipowsky and T. R. Weikl, *Adv Colloid Interface Sci*, 2014, **208**, 214-224.
95. C. Montis, D. Maiolo, I. Alessandri, P. Bergese and D. Berti, *Nanoscale*, 2014, **6**, 6452-6457.